

การเพิ่มประสิทธิภาพเซลล์แสงอาทิตย์ชนิดสีย้อมไวแสง

โดยการปรับปรุงชั้นไทเทเนียมไดออกไซด์อิเล็กโตรด



นาย กุลพงษ์ บุญยะเวศ

สถาบันวิทยบริการ

วิทยานิพนธ์นี้เป็นส่วนหนึ่งของการศึกษาตามหลักสูตรปริญญาวิศวกรรมศาสตรมหาบัณฑิต

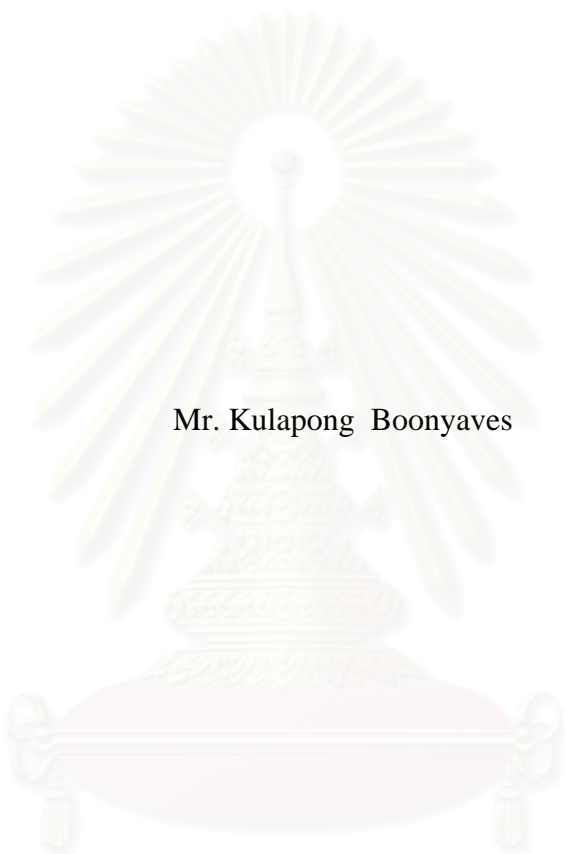
สาขาวิชาวิศวกรรมเคมี ภาควิชาวิศวกรรมเคมี

คณะวิศวกรรมศาสตร์ จุฬาลงกรณ์มหาวิทยาลัย

ปีการศึกษา 2549

ลิขสิทธิ์ของจุฬาลงกรณ์มหาวิทยาลัย

IMPROVING EFFICIENCY OF DYE-SENSITIZED SOLAR CELL
BY MODIFICATION OF TiO₂ ELECTRODE



Mr. Kulapong Boonyaves

สถาบันวิทยบริการ
จุฬาลงกรณ์มหาวิทยาลัย

A Thesis Submitted in Partial Fulfillment of the Requirements
for the Degree of Master of Engineering Program in Chemical Engineering

Department of Chemical Engineering

Faculty of Engineering


Chulalongkorn University

Academic Year 2006

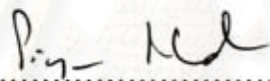
Copyright of Chulalongkorn University

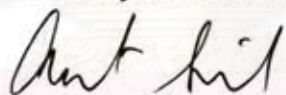
Thesis Title IMPROVING EFFICIENCY OF DYE-SENSITIZED
 SOLAR CELL BY MODIFICATION OF TiO₂ ELECTRODE
By Mr. Kulapong Boonyaves
Field of Study Chemical Engineering
Thesis Advisor Akawat Sirisuk, Ph.D.

Accepted by the Faculty of Engineering, Chulalongkorn University in Partial
Fulfillment of the Requirements for the Master's Degree

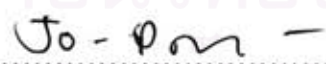

.....Dean of the Faculty of Engineering
(Professor Direk Lavansiri, Ph.D.)

THESIS COMMITTEE


.....Chairman
(Professor Piyasan Prasertdam, Dr.Ing.)


..... Thesis Advisor
(Akawat Sirisuk, Ph.D.)


..... Member
(Associate Professor Tawatchai Charinpanitkul, Ph.D.)



.....Member
(Assistant Professor Joongjai Panpranot, Ph.D.)

กุลพงษ์ บุญยะเวศ : การเพิ่มประสิทธิภาพเซลล์แสงอาทิตย์ชนิดสีย้อมไวแสง โดยการปรับปรุงชั้นไทเทเนียมไดออกไซด์อิเล็กโทรด (IMPROVING EFFICIENCY OF DYE-SENSITIZED SOLAR CELL BY MODIFICATION OF TiO_2 ELECTRODE) อ. ที่ปรึกษา: ดร.อัศวัต ศิริสุข, 72 หน้า

เซลล์แสงอาทิตย์ชนิดสีย้อมไวแสงถูกสร้างขึ้นโดยใช้ไทเทเนียมไดออกไซด์เป็นขั้วอิเล็กโทรด ในที่นี้การเตรียมชั้นฟิล์มไทเทเนียมไดออกไซด์ใช้เทคนิคการพ่นไทเทเนียมไดออกไซด์โพลีซึ่งเตรียมด้วยวิธีโพลีเจลด้วยเครื่องพ่นอัลตราโซนิค เริ่มแรกเป็นการศึกษาสภาวะแวดล้อมที่เหมาะสมสำหรับการเตรียมชั้นไทเทเนียมไดออกไซด์อิเล็กโทรด คือจำนวนชั้นการพ่นไทเทเนียมไดออกไซด์โพลี และอุณหภูมิการเผาไทเทเนียมไดออกไซด์ที่เหมาะสม จากการทดลองพบว่าการพ่นไทเทเนียมไดออกไซด์โพลีที่ 150 รอบ และการเผาไทเทเนียมไดออกไซด์ที่ 500 องศาเซลเซียส ให้ประสิทธิภาพของเซลล์แสงอาทิตย์ที่ดีที่สุด หลังจากนั้นชั้นฟิล์มไทเทเนียมไดออกไซด์ได้ถูกปรับปรุงโดยการเติมวานาเดียมและสแกนเดียม ผลการทดลองพบว่าจะทำให้ประสิทธิภาพของเซลล์แสงอาทิตย์ชนิดสีย้อมไวแสงลดลง หลังจากนั้นได้ปรับปรุงชั้นฟิล์มไทเทเนียมไดออกไซด์ด้วยการเติมสารประกอบทีซีเอ็นคิว แล้วนำไปเผาชั้นฟิล์มไทเทเนียมไดออกไซด์ที่อุณหภูมิ 250 องศาเซลเซียส พบว่าประสิทธิภาพของเซลล์แสงอาทิตย์จะดีขึ้น โดยมีประสิทธิภาพสูงสุดที่การเติม 2% (น้ำหนักทีซีเอ็นคิวต่อน้ำหนักไทเทเนียมไดออกไซด์) ในส่วนสุดท้าย หลังเติมสารประกอบทีซีเอ็นคิวแล้วทำการเผาชั้นไทเทเนียมไดออกไซด์ที่อุณหภูมิ 400 องศาเซลเซียส ซึ่งสูงกว่าอุณหภูมิในการสลายตัวของสารประกอบทีซีเอ็นคิว และทำให้เกิดช่องว่างขึ้นแทนที่สารประกอบทีซีเอ็นคิวเดิม ส่งผลให้ประสิทธิภาพของเซลล์แสงอาทิตย์ชนิดสีย้อมไวแสงดียิ่งขึ้น โดยประสิทธิภาพดีที่สุดในที่การเติม 9% ของน้ำหนักสารประกอบทีซีเอ็นคิวต่อน้ำหนักสารไทเทเนียมไดออกไซด์

สถาบันวิทยบริการ
จุฬาลงกรณ์มหาวิทยาลัย

ภาควิชา.....วิศวกรรมเคมี..... ลายมือชื่อนิสิต..... กุลพงษ์ บุญยะเวศ.....

สาขาวิชา.....วิศวกรรมเคมี..... ลายมือชื่ออาจารย์ที่ปรึกษา..... 

ปีการศึกษา.....2549.....

##4770223921: MAJOR CHEMICAL ENGINEERING

KEY WORD: DYE-SENSITIZED SOLAR CELL/TITANIUM (IV) DIOXIDE /
SPRAY TECHNIQUES/ TCNQ / THICKNESS/TEMPERATURE/ELECTROLYTE

KULAPONG BOONYAVES: IMPROVING EFFICIENCY OF DYE-
SENSITIZED SOLAR CELL BY MODIFICATION OF TiO₂ ELECTRODE

THESIS ADVISOR: AKAWAT SIRISUK, Ph.D. 72 pp.

Dye-sensitized solar cell (DSSC) was constructed using TiO₂ as anode electrode layer. TiO₂ electrode layer was prepared from ultrasonic spray coating of TiO₂ sol, which was synthesized from a sol-gel method. First, preparation parameters for TiO₂ electrode layer (i.e., number of coats of TiO₂ and sintering temperature) were varied. The highest efficiency for DSSC was obtained when the number of coats of TiO₂ was 150 and sintering temperature for TiO₂ layer was 150 °C. Next, TiO₂ electrode layer was modified by addition of scandium and vanadium, resulting in lower efficiency of DSSC. TiO₂ electrode layer was also modified by addition of tetracyanoquinodimethane (TCNQ). The solar cells with TCNQ modified TiO₂ electrode was sintered at 250°C and exhibited the highest efficiency at 2% (w/w) TCNQ in TiO₂. Finally, the solar cells with TCNQ modified TiO₂ electrode was sintered at 400°C, which exceeded decomposition temperature of TCNQ, resulting the presence of hollow spaces in place of TCNQ. The solar cells with TiO₂ electrode layer modified by hollow spaces exhibited the highest efficiency at initial concentration of TCNQ added of 9% (w/w) TCNQ in TiO₂.

สถาบันวิทยบริการ
จุฬาลงกรณ์มหาวิทยาลัย

Department.....Chemical Engineering..... Student's signature... *Kulapong B.*

Field of study....Chemical Engineering..... Advisor's signature... *Ant Sirisuk*

Academic year.....2006.....

ACKNOWLEDGEMENTS

This thesis would not have been possible to complete without the support of the following individuals. Firstly, I would like to express my greatest gratitude to my advisor, Dr. Akawat Sirisuk, for his invaluable guidance during the course of this work. And I am also very grateful to Professor Dr. Piyasan Praserthdam, for his kind supervision over this thesis as the chairman, Assistant Professor Tawatchai Charinpanitkul and Assistant Professor Joongjai Panpranot, members of the thesis committee for their kind cooperation.

The financial supports from Thailand Research Fund, Commission on Higher Education and Graduate School of Chulalongkorn University are also gratefully acknowledged.

Many thanks for kind suggestions and useful help to staffs of Nectec at NSTDA for solar simulation (I-V tester) and many friends in the Research Center on Catalysis and Catalytic Reaction Engineering who always provide the encouragement and assistance along the study.

Finally, I also would like to dedicate this thesis to my parents, my aunt and my sister who have always been the source of my support and encouragement.

สถาบันวิทยบริการ
จุฬาลงกรณ์มหาวิทยาลัย

CONTENTS

	Page
ABSTRACT (IN THAI).....	iv
ABSTRACT (IN ENGLISH).....	v
ACKNOWLEDGEMENTS.....	vi
CONTENTS.....	vii
LIST OF TABLES.....	x
LIST OF FIGURES.....	xi
CHAPTER	
I INTRODUCTION.....	1
II LITERATURE REVIEWS.....	4
2.1 Basic information about dye-sensitized solar cell (DSSC).....	4
2.2 Effect of electrolyte on efficiency of dye-sensitized solar cell ...	6
2.3 Effect of thickness and sintering temperature for TiO ₂ film on efficiency of dye-sensitized solar cell	7
III THEORY.....	8
3.1 The Basic of Solar Cell	8
3.1.1 Photons In, Electrons Out: Photovoltaic Effect.....	8
3.1.2 Brief History of the Solar Cell.....	9
3.1.3 Photovoltaic Cells and Power Generation.....	12
3.1.3.1 Photovoltaic cells, Modules and Systems.....	12
3.1.3.2 Some Important Definitions.....	14
3.1.4 Characteristics of the Photovoltaic Cell: A Summary.....	15
3.1.4.1 Photocurrent and Quantum efficiency.....	15
3.1.4.2 Dark current and open circuit voltage.....	17
3.1.4.3 Efficiency.....	19
3.1.4.4 Parasitic resistances.....	22
3.2 Dye Sensitized Solar Cell.....	24

3.3 Titanium dioxide.....	26
3.3.1 Physical and chemical properties.....	26
3.3.2 Applications of titanium dioxide.....	28
3.1.2 Sol-Gel Method	29
IV EXPERIMENTAL.....	30
4.1 Preparation of TiO ₂ sol and modified TiO ₂ sols	30
4.1.1 Preparation of TiO ₂ sol	30
4.1.2 Modification of TiO ₂ sol	30
4.1.2.1 Adding vanadium chloride	31
4.1.2.2 Adding scandium chloride	31
4.1.2.3 Adding tetracyanoquinodimethane (TCNQ)	31
4.2 Preparation of dye-sensitized solar cell components and the fabrication procedure.....	32
4.2.1 Dye	32
4.2.2 Electrolyte	32
4.2.2.1 Electrolyte I	32
4.2.2.2 Electrolyte II	33
4.2.3 Platinum counter electrode	33
4.2.4 TiO ₂ anode electrode	34
4.2.5 Fabrication of dye-sensitized solar cell assembly	36
4.3 Physical and Electrochemical Characterization	37
4.3.1 X-ray diffractometry (XRD).....	37
4.3.2 Nitrogen physisorption.....	37
4.3.2 Fourier transform infrared spectroscopy (FT-IR).....	37
4.3.4 Thermo gravimetric Analysis (TGA).....	38
4.3.5 Current-Voltage Tester (I-V Tester).....	38

V RESULTS AND DISSCUSSION.....	39
5.1 Effect of type of electrolyte.....	39
5.2 Effect of Sintering Temperature forTiO ₂ Electrode	41
5.3 Effect of Thickness of TiO ₂ Film	46
5.4 Effect of modification of TiO ₂ electrode layer	48
5.4.1 Modification of TiO ₂ electrode layer by scandium and vanadium.....	48
5.4.2 Modification of TiO ₂ electrode layer by adding TCNQ.....	54
5.4.3 Modification of TiO ₂ electrode layer with hollow spaces...	56
VI CONCLUSIONS AND RECOMMENDATIONS.....	61
6.1 Conclusions.....	61
6.2 Recommendations for future studies.....	62
REFERENCES.....	63
APPENDIX.....	67
APPENDIX A: CALCULATION OF THE FILL FACTOR AND EFFICIENCY OF DYE SENSITIZED SOLAR CELL.....	68
VITA.....	72

LIST OF TABLES

Table	Page
3.1 Performance of some types of PV cell	21
3.2 Comparison of rutile, brookite and anatase.....	27
4.1 Number of coats of TiO ₂ applied before each drying	35
5.1 Electrochemical properties of DSSC with different electrolyte	39
5.2 Physical properties of TiO ₂ powders as obtained from XRD and nitrogen adsorption.....	43
5.3 Electrochemical properties of DSSC of which TiO ₂ electrode was fired at various temperatures	43
5.4 Electrochemical properties of dye-sensitized solar cells with various thickness of TiO ₂ electrode layer	46
5.5 Physical data of doped TiO ₂ powders by XRD and nitrogen adsorption.....	51
5.6 Electrochemical properties of DSSC with TiO ₂ electrode layer modified by TCNQ at various concentrations.....	55
5.7 Electrochemical properties of DSSC with TiO ₂ electrode layer modified with hollow spaces derived from TCNQ	58


 สถาบันวิทยบริการ
 จุฬาลงกรณ์มหาวิทยาลัย

LIST OF FIGURES

Figure	Page
3.1 Comparison of the photoelectric effect (left), where uv light liberates electrons from the surface of a metal, with the photovoltaic effect in a solar cell (right). The photovoltaic cell needs to have some spatial asymmetry, such as contacts with different electronic properties, to drive the excited electrons through the external circuit.....	9
3.2 (a) Photovoltaic cell showing surface contact patterns (b) In a module, cells are usually connected in series to give a standard dc voltage of 12 V (c) For any application, modules are connected in series into strings and then in parallel into an array, which produces sufficient current and voltage to meet the demand. (d) In most cases the photovoltaic array should be integrated with components for charge regulation and storage.....	13
3.3 The solar cell may replace a battery in a simple circuit.....	14
3.4. Voltage-current curves of a conventional battery (grey) and a solar cell under different levels of illumination. A battery normally delivers a constant e.m.f. at different levels of current drain except for very low resistance loads, when the e.m.f. begins to fall. The battery e.m.f. will also deteriorate when the battery os heavily discharged. The solar cell delivers a constant current for any given illumination level while the voltage is determined largely by the resistance of the load. For photovoltaic cells it is usual to plot the data in the opposite sense, with current on the vertical axis and voltage on the horizontal axis. This is because the photovoltaic cell is essentially a current source, while the battery is a voltage source.....	16
3.5 Quantum efficiency of GaAs cell compared to the solar spectrim. The vertical scale is in arbitrary units, for comparison. The short circuit photocurrent is obtained by integrating the product of the photon flux density and QE over photon energy. It is desirable to have a high QE at wavelength where the solar flux density is high.....	16

Figure	Page
3.6 Current-voltage characteristic of ideal diode in the light and the dark. To a first approximation, the net current is obtained by shifting the bias dependent dark current up by a constant amount, equal to the short circuit photocurrent. The sign convention is such that the short circuit photocurrent is positive.....	18
3.7 Equivalent circuit of ideal solar cell.....	19
3.8 The current voltage (black) and power-voltage (grey) characteristics of an ideal cell. Power density reaches a maximum at a bias V_m , close to V_{oc} . The maximum power density $J_m \times V_m$ is given by the area of the inner rectangle. The outer rectangle has area $J_{sc} \times V_{oc}$. If the fill factor were equal to 1, the current voltage curve would follow the outer rectangle.....	20
3.9 Plot of J_{sc} against V_{oc} for the cells listed in Table 1.1. Materials with high V_{oc} tend to have lower J_{sc} . This is due to the band gap of the semiconductor material. The grey line shows the relationship expected in the theoretical limit.....	22
3.10 Equivalent circuit including series and shunt resistances.....	22
3.11 Effect of (a) increasing series and (b) rebuking parallel resistances. In each case the outer curve has $R_s = 0$ and $R_{sh} = \infty$. In each case the effect of the resistance is to reduce the area of the maximum power rectangle compared to $J_{sc} \times V_{oc}$	23
3.12 Dye solar cell in which the electron-hole pairs are produced in a ruthenium bipyridil dye. The electrons flow outwards towards the left through the n-conductor TiO_2 and the holes towards the right through the iodine ions with which the acetonitrile electrolyte is doped.....	25
4.1. Schematic diagram of a platinum counter electrode	33
4.2. Show anode electrode before sprayed	34
4.3 Dye-sensitized solar cell assembly before electrolyte injection	36
4.4. Arrangement of various layers within dye-sensitized solar cell assembly ...	36
5.1 I-V curves of DSSC with (a) Electrolyte I and (b) Electrolyte II	40

Figure	Page
5.2 Results from XRD for TiO ₂ powders that were fired at, (a) 200 °C, (b) 300 °C, (c) 400 °C, and (d) 500 °C	42
5.3 Efficiency of DSSC as a function of sintering temperature of DSSC	44
5.4 I-V curve of dye-sensitized solar cell, of which TiO ₂ electrode layer was fired at 500 °C.	45
5.5 Efficiency of DSSC as a function of number of coats of TiO ₂ for the electrode	47
5.6 The periodic table that contains scandium, titanium and scandium	48
5.7 XRD results for TiO ₂ powder modified with (a) 0%(w/w), (b) 2%(w/w), (c) 5%(w/w), and (d) 9%(w/w) of scandium.	49
5.8 XRD results for TiO ₂ powder modified with (a) 0%(w/w), (b) 2%(w/w), (c) 5%(w/w), and (d) 9%(w/w) of vanadium	50
5.9 Efficiencies of dye-sensitized solar cells with TiO ₂ electrode layer modified by scandium at various concentrations.....	52
5.10 Efficiencies of dye-sensitized solar cells with TiO ₂ electrode layer modified by vanadium at various concentrations	53
5.11 Result from thermogravimetric analysis (TGA) for TCNQ in air.....	54
5.12 Efficiency of dye-sensitized solar cell with TiO ₂ electrode layer modified by TCNQ at various concentrations	56
5.13 Results from TGA for TiO ₂ powders that modified by adding TCNQ at (a) 0%, (b) 2%, (c) 5%, and (d) 9% (w/w). The TiO ₂ powders were then fired at 400°C.....	57
5.14 Results from FT-IR for TiO ₂ powders that modified by adding TCNQ at (a) 0%, (b) 2%, (c) 5%, and (d) 9% (w/w). The TiO ₂ powders were then fired at 400°C.....	58
5.15 Efficiency of dye-sensitized solar cell with TiO ₂ electrode layer modified by hollow spaces at various concentrations.....	59
5.16 Schematic diagram of improved performance of DSSC with TiO ₂ electrode layer modified by adding hollow spaces.....	60

Figure	Page
A.1 An I-V curve of DSSC with 150 coats of TiO_2 that is sintered at 400°C	69
A.2 An I-V curve of DSSC with 180 coats of TiO_2 that is sintered at 500°C	70
A.3 An I-V curve of DSSC with 180 coats of TiO_2 that is sintered at 500°C . A new rectangle is drawn in order to cover the shaded area.....	71



สถาบันวิทยบริการ
จุฬาลงกรณ์มหาวิทยาลัย

CHAPTER I

INTRODUCTION

Titanium dioxide (TiO_2), or titania, is widely used in many applications such as photocatalysis, self-cleaning surface, UV absorber, pigment and gas sensor. Major applications of TiO_2 involve photocatalytic oxidation using TiO_2 as the photocatalyst which has been studied by several researchers (Sirisuk et al., 1999; Fu et al., 1996; Park et al., 1999). Those observed different catalyst activities and efficiencies for TiO_2 that was prepared differently.

Dye-sensitized solar cells (DSSC) have been attracting considerable attention all over the world because of their reasonable conversion efficiency, low production cost and simple fabrication process when compared to silicon solar cells (O'Regan et al., 1991). The photochemical solar cell consists of a transparent and conducting fluorine-doped tin oxide (FTO) coated with nanocrystalline thin film of TiO_2 as an anodic material, where ruthenium(II) complex dye molecules are chemisorbed on the surface of semiconductor through functional anchoring groups such as carboxylic or phosphonic acid (Kalyanasundaram et al., 1998). The pores of TiO_2 are filled with an electrolyte containing I^-/I_3^- redox couple. A platinum coated FTO material is used for the completion of the electrical circuit. The overall mechanism involves the light absorption by the dye molecules resulting in the rapid injection of electrons to the conduction band of the TiO_2 . The adsorbed dye is regenerated to its original state by electron transfer from tri-iodide ions (I_3^-) present in the electrolyte, which are in turn reduced at the counter-electrode (Rothenberger et al., 1999). In DSSC research, nanosized TiO_2 materials have attracted much attention as a semiconductor material because of their unusual physical and chemical properties (Gratzel et al., 2004). By using a nanocrystalline-based TiO_2 electrode, the surface area can be increased to about 2,000 times compared with flat layered electrode (Schlaf et al., 1999).

Typically, titania electrode layer for dye sensitized solar cell is prepared by screen printing or coating technique, which titania powders are mixed with binder and solvent and the paste is then coated on a conducting glass. The screen printing or coating paste can produce thin film of titania easily, but the drawbacks are difficulty in controlling thickness of film and the presence of binder in an electrode layer, binder such as polymer which may hinder electron transfer.

TiO₂ can be synthesized via a number of techniques, including precipitation, chemical vapor deposition, solvothermal method and glycothermal method. One of the techniques used for synthesis of titania is a sol-gel method. This technique can produce nanosized titania at room temperature without consuming a great deal of energy.

Ultrasonic spray coating is a relatively new technology for coating, which can produce smooth film and can control film thickness rather easily. This technique can be employed to produce titania electrode layer by using titania sol. Binder is not necessary in this case.

Cis-di(thiocyanate)bis(2,2'-bipyridine-4,4'-dicarboxylate)ruthenium(II) or N3 dye (R535) is the dye that is popularly employed in DSSC and was used in this study. The electrolyte that we choose for comparison are a mixture composed of 0.6 M dimethylpropylimidazolium iodide, 0.1 M LiI, 0.05 M I₂, 0.5 M tert-butylpyridine in acetonitrile and a mixture composed of 0.5 M LiI, 0.05 M I₂, 0.5 M tert-butylpyridine in acetonitrile. Conducting glass was purchased from a commercial source. Platinum counter electrode was prepared by sputtering.

The objectives of this research are as follows.

1. To study principles involving dye-sensitized solar cell and assemble the solar cell
2. To optimize conditions for preparation of titania electrode layer such as film thickness and calcinations temperature to maximize efficiency of the dye-sensitized solar cell.
3. To improve efficiency of electron transfer process in dye-sensitized solar cell by adding other compounds to modify TiO_2 layer, which is the anode electrode and study the effects of the modification on physical and electrochemical properties of the TiO_2 layer.

This thesis is arranged as follows.

Chapter I present the introduction of this study.

Chapter II presents literature reviews of previous works related to this research.

Chapter III explains basic principles of solar cell and dye-sensitized solar cell, basic information about TiO_2 and preparation of TiO_2 via a sol-gel method.

Chapter IV describes synthesis of the TiO_2 sol and modified TiO_2 sol, preparation of dye-sensitized solar cell and the fabrication procedure, and characterization techniques used in this study.

Chapter V describes experimental results and discussion of this research.

Chapter VI presents overall conclusions of this research and recommendations for future work.

CHAPTER II

LITERATURE REVIEWS

This chapter presents the literature reviews performed prior to the beginning of experimental works. This chapter contained basic information regarding dye-sensitized solar cell (DSSC), the effect of electrolyte for DSSC, the effect of thickness and calcinations temperature for TiO₂ electrode layer.

2.1 Basic information about dye-sensitized solar cell (DSSC)

Ramasamy and coworkers (2006) prepared DSSC by using screen-printing technology, which was used to fabricate large DSSC. The high series-resistance associated with transparent conductive oxide glass substrates caused poor performance in large DSSC, especially at an exposure of one sun. The DSSC design had an embedded silver grid, a fluorine-doped tin oxide (FTO) glass substrate, and stripe-type titanium dioxide active layers introduced by screen-printing. The counter electrode was prepared from a screen printable paste based on hexachloro platinum acid. A DSSC module, which consisted of five stripe-type working electrodes on a 5 cm×5 cm, embedded silver grid FTO glass substrate, exhibited stable performance with an energy conversion efficiency of 5.45% under standard test conditions.

Karthikeyan and coworkers (2006) stated that the nature and morphology of titanium dioxide films played a significant role in determining the overall efficiency of the DSSC. They studied three different nanocrystalline titania films, prepared from three different routes, namely sol-gel (FMF), thermal (P-25), and colloidal-microwave processes (CMP). Different preparation of nanotitania led to different surface areas, pore sizes and morphologies of the mesoporous films. FMF-TiO₂ displayed the highest efficiency and incident photon to current conversion (IPCE) in DSSC among the three because it possessed pure anatase phase; optimum surface area, pore volume and pore

diameter; and well-connected network of individual nanoparticles. P-25 films exhibited pore structural and morphological features similar to FMF films but displayed lower efficiency than FMF-TiO₂ due to the presence of small percentage of rutile phase besides major anatase phase. Although, CMP films had high surface area, it possessed smaller pore diameter and pore volume in addition to agglomerates and macropores, leading to lower efficiency. Therefore, the optimal pore and morphological structures were necessary for efficient functioning of solid-state dye sensitised solar cell.

Kim and coworkers (2006) prepared titan nanotubes by hydrothermal process using commercial titania nanoparticles. Subsequently, the titanate nanotubes film was fabricated at room temperature on FTO substrates using electrophoretic deposition (EPD) method at 40 V. The average lengths of these nanotubes were few hundreds of nanometers and the diameters were 10–20 nm, with reasonably dense and uniform film. During EPD, the intercalated sodium from the titanate nanotubes was removed, as confirmed by XRD and EDX. Finally, after annealing the film at a temperature between 450 °C and 550 °C, DSSC were prepared from two types of the films fabricated by electrophoretic deposition and doctor-blade method. The open circuit voltage (V_{oc}) in all the cases was 0.8 V, with incident radiation intensity adjusted to AM-1.5. The solar cell made from electrodeposited titanate nanotubes annealed at 500 °C showed a photocurrent density (I_{sc}) of 15.67 mA/cm². The solar cell fabricated with doctor-blade method using titanate nanotubes, annealed at 450 °C shows much lower photocurrent density 1.31 mA/cm².

Bandara and Weerasinghe (2005) investigated dye-sensitized solar cells consisted of thin layer of p-type NiO on TiO₂. The thin NiO layer acted as a hole collector as well as a barrier for charge recombination. The p-type oxide materials could be used to construct dye-sensitized solar cells successfully.

Ngamsinlapasathian and coworkers (2004) prepared an electrode for dye-sensitized solar cell using titania that contained nanotube (TiNT) structure. To obtain highly efficient cell, the thickness of TiNT electrode must be increased to attain high amount of dye. TiNT +2%P25 was the most suitable composition to obtain well-balanced properties.

Shen and coworkers (2004) compared four types of nanostructured titanium dioxide electrodes with nanocrystalline particles of different sizes (15 and 27 nm in diameter) and with the addition of polyethylene glycol binders having two different molecular weights (20,000 and 500,000). CdSe nanoparticles were adsorbed onto each of the four types of TiO₂ electrode. The photoelectrochemical current and incident photon to current conversion efficiency were strongly dependent on the size of TiO₂ nanoparticles and the molecular weight of PEG in the TiO₂/water paste.

2.2 Effect of electrolyte on efficiency of dye-sensitized solar cell

Suri and coworkers (2006) studied the effect of electrolytes on the photovoltaic performance of hybrid dye sensitized ZnO solar cells based on Eosin Y dye. The efficiency of DSSC depended on a number of factors such as impedance from anions in the electrolytes, oxidation–reduction process of anions and size of cations of the electrolyte. The size of the cations was varied by choosing different electrolytes such as LiBr+Br₂, LiI+I₂, tetrapropylammonium iodide +I₂ in mixed solvent of acetonitrile and ethylene carbonate. The impedance of anions was determined by electrochemical impedance spectra. Br⁻/Br₃⁻ offers as high an impedance as I⁻/I₃⁻ couple. The oxidation–reduction reactions of electrolytes were measured by linear sweep voltammogram. Br⁻/Br₃⁻ was more suitable than an I⁻/I₃⁻ couple in DSSC in terms of higher open-circuit photovoltage production and higher overall energy conversion efficiency. This was attributed to more positive potential of the dye sensitizer than that of Br⁻/Br₃⁻. The gain in V_{oc} was due to the enlarged energy level difference between the redox potential of the electrolyte and the Fermi level of ZnO and the suppressed charge recombination as well.

Hara and coworkers (2004) investigated the influence of electrolyte composition on the photovoltaic performance of a dye-sensitized nanocrystalline TiO₂ solar cell (DSSC) based on a Ru(II) terpyridyl complex photosensitizer (the black dye). The interaction between the electrolyte components and the adsorbed dye was investigated spectroscopically. The absorption peaks that were attributed to the metal-to-ligand charge transfer transitions of the black dye in solution and adsorbed on a TiO₂ film were red-shifted in the presence of Li cations, leading to an expansion of the spectral response of the solar cell toward the near-IR region. The photovoltaic performance of the DSSC based on the black dye depended remarkably on the electrolyte composition. They developed a novel efficient organic liquid electrolyte containing an imidazolium iodide such as 1,2-dimethyl-3-n-propylimidazolium iodide or 1-ethyl-3-methylimidazolium iodide (EMImI) for a DSSC based on the black dye.

2.3 Effect of thickness and sintering temperature for TiO₂ film on efficiency of dye-sensitized solar cell

Huang and coworker (2006) studied the effects of hydrothermal temperature on the preparation of TiO₂ colloids, and the effects of their film thickness on fluorine-doped tin oxide (FTO) glass, toward the performance of a DSSC were investigated. Pore diameter and surface area of the TiO₂ were of paramount importance in determining the cell efficiency. With an increase in hydrothermal temperature, the pore diameter increased linearly. However, the surface area showed the reverse effect. The DSSC assembled with the TiO₂ films prepared under the hydrothermal temperature of 240 °C with the thickness larger than 10 nm gave optimal performance. The effect of film thickness of TiO₂ on the performance of the DSSC could be explained by the relative size of reactive species diffusing into the thin film and the lifetime of injected electrons. Electrochemical impedance spectroscopy was also used to analyze the resistance of the cell, developed as a result of the change in the thickness of the TiO₂ thin film. The at-rest stability for over 200 days was monitored and the results showed that the solar energy conversion efficiency was found to decrease from 5.0% of initial value to 3.0% at the end.

CHAPTER III

THEORY

This chapter presents basic knowledge about solar cell and dye-sensitized solar cell. The last section gives basic information about titanium dioxide.

3.1. The Basic of Solar Cell

This section contains excerpts from a book by Jenny Nelson [2004].

3.1.1 Photons In, Electrons Out: The Photovoltaic Effect

Solar photovoltaic energy conversion is a one-step conversion process which generates electrical energy from light energy. The explanation relies on ideas from quantum theory. Light is made up of packets of energy, called photons, whose energy depends only upon the frequency, or colour, of the light. The energy of visible photons is sufficient to excite electrons, bound into solids, up to higher energy levels where they are more free to move. An extreme example of this is the photoelectric effect, the celebrated experiment which was explained by Einstein in 1905, where blue or ultraviolet light provides enough energy for electrons to escape completely from the surface of a metal. Normally, when light is absorbed by matter, photons are given up to excite electrons to higher energy states within the material, but the excited electrons quickly relax back to their ground state. In a photovoltaic device,

However, there is some built-in asymmetry which pulls the excited electrons away before they can relax, and feeds them to an external circuit. The extra energy of the excited electrons generates a potential difference, or electromotive force (e.m.f). This force drives the electrons through a load in the external circuit to do electrical work.

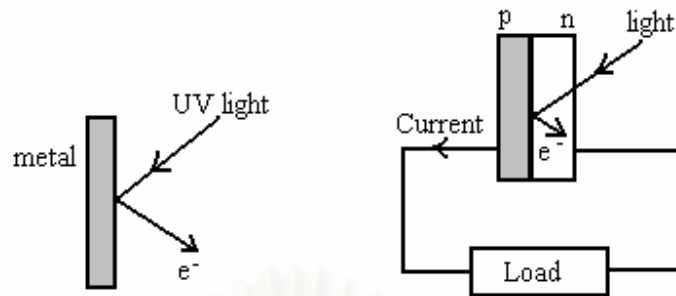


Figure 3.1 Comparison of the photoelectric effect (left), where uv light liberates electrons from the surface of a metal, with the photovoltaic effect in a solar cell (right). The photovoltaic cell needs to have some spatial asymmetry, such as contacts with different electronic properties, to drive the excited electrons through the external circuit.

The effectiveness of a photovoltaic device depends upon the choice of light absorbing materials and the way in which they are connected to the external circuit. The following chapters will deal with the underlying physical ideas, the device physics of solar cell, the properties of photovoltaic materials and solar cell design. In this chapter we will summarize the main characteristics of a photovoltaic cell without discussing its physical function in detail.

3.1.2. Brief History of the Solar Cell

The photovoltaic effect was first reported by Edmund Becquerel in 1839 when he observed that the action of light on a silver coated platinum electrode immersed in electrolyte produced an electric current. Forty years later the first solid state photovoltaic devices were constructed by workers investigating the recently discovered photoconductivity of selenium. In 1876 William Adams and Richard Day found that a photocurrent could be produced in a sample of selenium when contacted by two heated platinum contacts. The photovoltaic action of the selenium differed from its photoconductive action in that a current was produced spontaneously by the action of light. No external power supply was needed. In this early photovoltaic device, a rectifying junction had been formed between the semiconductor and the metal contact. In

1894, Charles Fritts prepared what was probably the first large area solar cell by pressing a layer of selenium between gold and another metal. In the following years photovoltaic effects were observed in copper-copper oxide thin film structure, in lead sulphide and thallium sulphide. These early cells were thin film Schottky barrier devices, where a semitransparent layer of metal deposited on top of the semiconductor provided both the asymmetric electronic junction, which is necessary for photovoltaic action, and access to the junction for the incident light. The photovoltaic effect of structures like this was related to the existence of a barrier to current flow at one of the semiconductor-metal interfaces (i.e., rectifying action) by Goldman and Brodsky in 1914. Later, during the 1930s, the theory of metal-semiconductor barrier layers was developed by Walter Schottky, Neville Mott and others.

However, it was not the photovoltaic properties of materials like selenium which excited researchers, but the photoconductivity. The fact that the current produced was proportional to the intensity of the incident light, and related to the wavelength in a definite way meant that photoconductive materials were ideal for photographic light meters. The photovoltaic effect in barrier structures was an added benefit, meaning that the light meter could operate without a power supply. It was not until the 1950s, with the development of good quality silicon wafers for applications in the new solid state electronics, that potentially useful quantities of power were produced by photovoltaic devices in crystalline silicon.

In the 1950s, the development of silicon electronics followed the discovery of a way to manufacture p-n junctions in silicon. Naturally n type silicon wafers developed a p type skin when exposed to the gas boron trichloride. Part of the skin could be etched away to give access to the n type layer beneath. These p-n junction structure produced much better rectifying action than Schottky barriers, and better photovoltaic behaviors. The first silicon solar cell was reported by Chapin, Fuller and Pearson in 1954 and converted sunlight with an efficiency of 6%, six times higher than the best previous attempt. That figure was to rise significantly over the following years and decades but, at an estimated production cost of some 200 per Wat, these cells were not seriously

considered for power generation for several decades. Nevertheless, the early silicon solar cell did introduce the possibility of power generation in remote locations where fuel could not easily be delivered. The obvious application was to satellites where the requirement of reliability and low weight made the cost of the cells unimportant and during the 1950s and 60s, silicon solar cells were widely developed for applications in space.

Also in 1954, a cadmium sulphide p-n junction was produced with an efficiency of 6%. And in the following years studies of p-n junction photovoltaic devices in gallium arsenide, indium phosphide and cadmium telluride were stimulated by theoretical work indicating that these materials would offer a higher efficiency. However, silicon remained and remains the foremost photovoltaic material, benefiting from the advances of silicon technology for the microelectronics industry. Short histories of the solar cell are given elsewhere [Shive,1959; Wolf,1972; Green, 1990]

In the 1970s the crisis in energy supply experienced by the oil-dependent western world led to a sudden growth of interest in alternative sources of energy, and funding for research and development in those areas. Photovoltaics was a subject of intense interest during this period, and a range of strategies for producing photovoltaic devices and materials more cheaply and for improving device efficiency were explored. Routes to lower cost included photoelectrochemical junctions, and alternative materials such as photocrystalline silicon, amorphous silicon, other 'thin film' materials and organic conductors. Strategies for higher efficiency included tandem and other multiple band gap designs. Although none of these led to widespread commercial development, our understanding of the science of photovoltaics is mainly rooted in this period.

During the 1990s, interest in photovoltaics expanded, along with growing awareness of the need to secure sources of electricity alternative to fossil fuels. The trend coincides with the widespread deregulation of the electricity markets and growing recognition of the viability of decentralized power. During this period, the economics of photovoltaics improved primarily through economies of scale. In the late 1990s the

photovoltaic production expanded at a rate of 15-25% per annum, driving a reduction in cost. Photovoltaics first became competitive in contexts where conventional electricity supply is most expensive, for instance, for remote low power applications such as navigation, telecommunications, and rural electrification and for enhancement of supply in grid-connected loads at peak use [Anderson, 2001]. As prices fall, new markets are opened up. An important example is building integrated photovoltaic applications, where the cost of the photovoltaic system is offset by the savings in building materials.

3.1.3 Photovoltaic Cells and Power Generation

3.1.3.1. Photovoltaic cells, Modules and Systems

The solar cell is the basic building block of solar photovoltaics. The cell can be considered as a two terminal device which conducts like a diode in the dark and generates a photovoltage when charged by the sun. Usually it is a thin slice of semiconductor material of around 100 cm^2 in area. The surface is treated to reflect as little visible light as possible and appears dark blue or black. A pattern of metal contacts is imprinted on the surface to make electrical contact (Fig. 3.2 (a)).

When charged by the sun, this basic unit generates a dc photovoltage of 0.5 to 1 volt and, in short circuit, a photocurrent of some tens of milliamps per cm^2 . Although the current is reasonable, the voltage is too small for most applications. To produce useful dc voltages, the cells are connected together in series and encapsulated into modules. A module typically contains 28 to 36 cells in series,

To generate a dc output voltage of 12 V in standard illumination conditions (Fig. 3.2 (b)). The 12 V modules can be used singly, or connected in parallel and series into an array with a larger current and voltage output, according to the power demanded by the application (Fig. 3.2 (c)). Cells within a module are integrated with bypass and blocking diodes in order to avoid the complete loss of power which would result if one cell in the

series failed. Modules within arrays are similarly protected. The array, which is also called a photovoltaic generator, is designed to generate power at a certain current and a

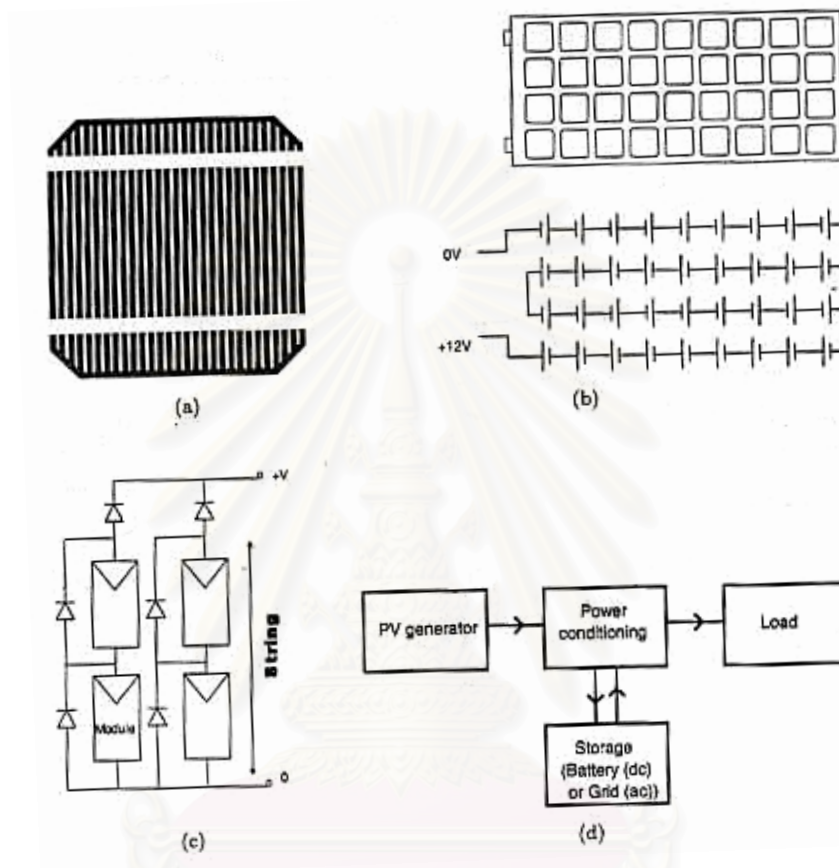


Figure 3.2 (a) Photovoltaic cell showing surface contact patterns (b) In a module, cells are usually connected in series to give a standard dc voltage of 12 V (c) For any application, modules are connected in series into strings and then in parallel into an array, which produces sufficient current and voltage to meet the demand. (d) In most cases the photovoltaic array should be integrated with components for charge regulation and storage

voltage which is some multiple of 12 V, under standard illumination. For almost all applications, the illumination is too variable for efficient operation all the time and the photovoltaic generator must be integrated with a charge storage system (a battery) and with components for power regulation (Fig. 3.2 (d)). The battery is used to store charge generated during sunny periods and the power conditioning ensures that the power supply

is regular and less sensitive to the solar irradiation. For ac electrical power, to power ac designed appliances and for integration with an electricity grid, the dc current supplied by the photovoltaic modules is converted to ac power of appropriate frequency using an inverter.

3.1.3.2 Some Important Definitions

The solar cell can take the place of a battery in a simple electric circuit (Fig. 3.3). In the dark the cell in circuit A does nothing. When it is switched on by light it develops a voltage, or e.m.f., analogous to the e.m.f. of the battery in circuit B. The voltage developed when the terminals are isolated (infinite load resistance) is called the open circuit voltage V_{oc} . The current drawn when the terminals are connected together is the short circuit current I_{sc} . For any intermediate load resistance R_L the cell develops a voltage V between 0 and V_{oc} and delivers a current I such that $V = IR_L$ and $I(V)$ is determined by the current-voltage characteristic of the cell under that illumination.



Figure 3.3 The solar cell may replace a battery in a simple circuit.

Thus both I and V are determined by the illumination as well as the load. Since the current is roughly proportional to the illuminated area, the short circuit current density J_{sc} is the useful quantity for comparison. These quantities are defined for a simple, ideal diode model of a solar cell in Sec. 3.4 below.

3.1.4 Characteristics of the Photovoltaic Cell: A Summary

3.1.4.1. Photocurrent and Quantum efficiency

The photocurrent generated by a solar cell under illumination at short circuit is dependent on the incident light. To relate the photocurrent density, J_{sc} , to the incident spectrum we need the cell's quantum efficiency, (QE). $QE(E)$ is the probability that an incident photon of energy E will deliver one electron to the external circuit. Then

$$J_{sc} = q \int b_s(E) QE(E) dE \quad (3.1)$$

Where $b_s(E)$ is the incident spectral photon flux density, the number of photons of energy in the range E to $E+dE$ which are incident on unit area in unit time and q is the electronic charge. QE depends upon the absorption coefficient of the solar cell material, the efficiency of charge separation and the efficiency of charge collection in the device but does not depend on the incident spectrum. It is therefore a key quantity in describing solar cell performance under different conditions. Figure 1.5 shows a typical QE spectrum in comparison with the spectrum of solar photons.

QE and spectrum can be given as functions of either photon energy or wavelength. Energy is a more convenient parameter for the physics of solar cells and it will be used in this book. The relationship between E and wavelength is defined by

$$E = \frac{hc}{\lambda} \quad (3.2)$$

Where h is Planck's constant and c the speed of light in vacuum. A convenient rule for converting between photon energies, in electron-Volts, and wavelength, in nm, is $E/eV = 1240/(\text{wavelength}/\text{nm})$

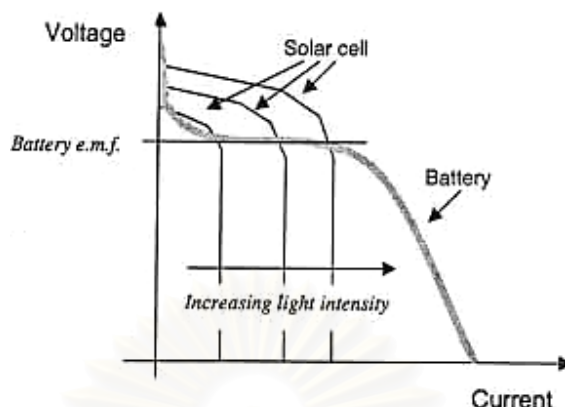


Figure 3.4. Voltage-current curves of a conventional battery (grey) and a solar cell under different levels of illumination. A battery normally delivers a constant e.m.f. at different levels of current drain except for very low resistance loads, when the e.m.f. begins to fall. The battery e.m.f. will also deteriorate when the battery is heavily discharged. The solar cell delivers a constant current for any given illumination level while the voltage is determined largely by the resistance of the load. For photovoltaic cells it is usual to plot the data in the opposite sense, with current on the vertical axis and voltage on the horizontal axis. This is because the photovoltaic cell is essentially a current source, while the battery is a voltage source.

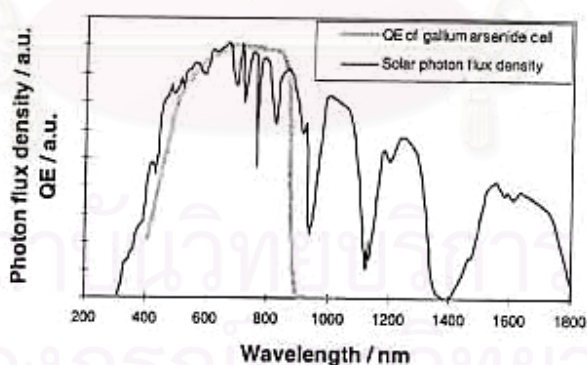


Figure 3.5 Quantum efficiency of GaAs cell compared to the solar spectrum. The vertical scale is in arbitrary units, for comparison. The short circuit photocurrent is obtained by integrating the product of the photon flux density and QE over photon energy. It is desirable to have a high QE at wavelength where the solar flux density is high.

3.1.4.2. Dark current and open circuit voltage

When a load is present, a potential difference develops between the terminals of the cell. This potential difference generates a current which acts in the opposite direction to the photocurrent, and the net current is reduced from its short circuit value. This reverse current is usually called the dark current in analogy with the current I_{dark} (V) which flows across the device under an applied voltage, or bias, V in the dark. Most solar cells behave like a diode in the dark, admitting a much larger current under forward bias ($V > 0$) than under reverse bias ($V < 0$). This rectifying behaviour is a feature of photovoltaic devices, since an asymmetric junction is needed to achieve charge separation. For an ideal diode the dark current density I_{dark} (V) varies like

$$J_{\text{dark}}(V) = J_0 (e^{qV/k_B T} - 1) \quad (3.3)$$

Where J_0 is a constant, k_B is Boltzmann's constant and T is temperature in degrees Kelvin.

The overall current voltage response of the cell, its current-voltage characteristic, can be approximated as the sum of the short circuit photocurrent and the dark current (Fig. 3.6). This step is known as the superposition approximation. Although the reverse current which flows in response to voltage in an illuminated cell is not formally equal to the current which flows in the dark, the approximation is reasonable for many photovoltaic materials and will be used for the present discussion.

The sign convention for current and voltage in photovoltaics is such that the photocurrent is positive. This is the opposite to the usual convention for electronic devices. With this sign convention the net current density in the cell is

$$J(V) = J_{SC} - J_{\text{dark}}(V), \quad (3.4)$$

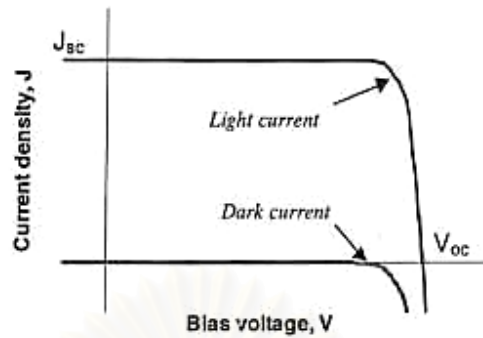


Figure 3.6 Current-voltage characteristic of ideal diode in the light and the dark. To a first approximation, the net current is obtained by shifting the bias dependent dark current up by a constant amount, equal to the short circuit photocurrent. The sign convention is such that the short circuit photocurrent is positive.

This becomes, for an ideal diode,

$$J = J_{sc} - J_0(e^{qV/k_B T} - 1) \quad (3.5)$$

When the contacts are isolated, the potential difference has its maximum value, the open circuit voltage V_{oc} . This is equivalent to the condition when the dark current and short circuit photocurrent exactly cancel out. For the ideal diode, from Eq. 3.5,

$$V_{oc} = \frac{kT}{q} \ln\left(\frac{J_{sc}}{J_0} + 1\right) \quad (3.6)$$

Equation 3.6 shows that V_{oc} increases logarithmically with light intensity. Note that voltage is defined so that the photovoltage occurs in forward bias, where $V > 0$.

Figure 3.6 shows that the current-voltage product is positive, and the cell generates power, when the voltage is between 0 and V_{oc} . At $V < 0$, the illuminated device acts as a photodetector, consuming power to generate a photocurrent which is light dependent but bias independent. At $V > V_{oc}$, the device again consumes power. This is the

regime where light emitting diodes operate. We will see later that in some materials the dark current is accompanied by the emission of light.

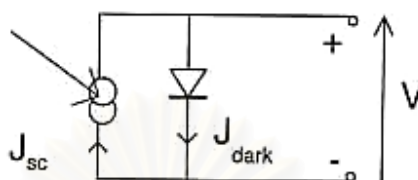


Figure 3.7 Equivalent circuit of ideal solar cell.

Electrically, the solar cell is equivalent to a current generator in parallel with an asymmetric, non linear resistive element, i.e., a diode (Fig. 1.7). When illuminated, the ideal cell produces a photocurrent proportional to the light intensity. That photocurrent is divided between the variable resistance of the diode and the load, in a ratio which depends on the resistance of the load and the level of illumination. For higher resistances, more of the photocurrent flows through the diode, resulting in a higher potential difference between the cell terminals but a smaller current through the load. The diode thus provides the photovoltage. Without the diode, there is nothing to drive the photocurrent through the load.

3.1.4.3. Efficiency

The operating regime of the solar cell is the range of bias, from 0 to V_{oc} , in which the cell delivers power. The cell power density is given by

$$P = JV. \quad (3.7)$$

P reaches a maximum at the cell's operating point or maximum power point. This occurs at some voltage V_m with a corresponding current density J_m , shown in Fig. 1.8 The optimum load thus has sheet resistance given by V_m/J_m . The fill factor is defined as the ratio

$$FF = \frac{J_m V_m}{J_{sc} V_{oc}} \quad (3.8)$$

And describes the ‘squareness’ of the J-V curve.

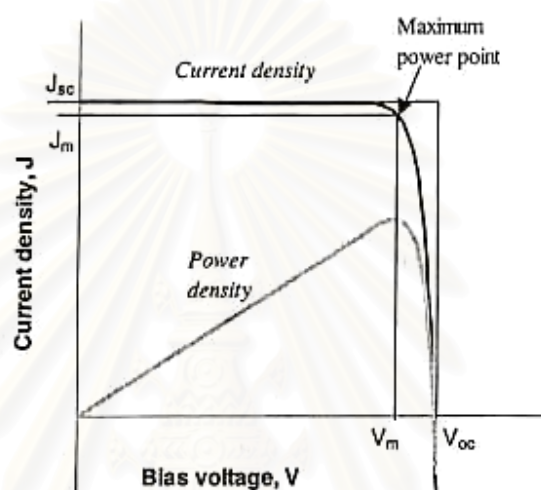


Figure 3.8 The current voltage (black) and power-voltage (grey) characteristics of an ideal cell. Power density reaches a maximum at a bias V_m , close to V_{oc} . The maximum power density $J_m \times V_m$ is given by the area of the inner rectangle. The outer rectangle has area $J_{sc} \times V_{oc}$. If the fill factor were equal to 1, the current voltage curve would follow the outer rectangle.

The efficiency η of the cell is the power density delivered at operating point as a fraction of the incident light power density, P_s ,

$$\eta = \frac{J_m V_m}{P_s} \quad (3.9)$$

Efficiency is related to J_{sc} and V_{oc} using FF,

$$\eta = \frac{J_{sc} V_{oc} FF}{P_s}. \quad (3.10)$$

These four quantities: J_{sc} , V_{oc} , FF and η are the key performance characteristics of a solar cell. All of these should be defined for particular illumination conditions. The Standard Test Condition (STC) for solar cells is the Air Mass 1.5 spectrum, an incident power density of 1000 Wm^{-2} , and a temperature of $25 \text{ }^\circ\text{C}$. The performance characteristics for the most common solar cell materials are listed in Table 3.1.

Table 3.1 shows that solar cell materials with higher J_{sc} tend to have lower V_{oc} . This is a consequence of the material used, and particularly of the band gap of the semiconductor.

Table 3.1 Performance of some types of PV cell [Green et al., 2001]

<i>Cell Type</i>	<i>Area (cm²)</i>	<i>V_{oc} (V)</i>	<i>J_{sc} (mA/cm²)</i>	<i>FF</i>	<i>Efficiency (%)</i>
Crystalline Si	4.0	0.706	42.2	82.8	24.7
Crystalline GaAs	3.9	1.022	28.2	87.1	25.1
Poly-Si	1.1	0.654	38.1	79.5	19.8
a-Si	1.0	0.887	19.4	74.1	12.7
CuInGaSe ₂	1.0	0.669	35.7	77.0	18.4
CdTe	1.1	0.848	25.9	74.5	16.4

Figure 3.9 illustrates the correlation between J_{sc} and V_{oc} for the cells in table 3.1, Together with the relationship for a cell of maximum efficiency.

3.1.4.4. Parasitic resistances

In real cells power is dissipated through the resistance of the contacts and through leakage currents around the sides of the device. The effects are equivalent electrically to two parasitic resistances in series (R_s) and in parallel (R_{sh}) with the cell (Fig. 3.10).

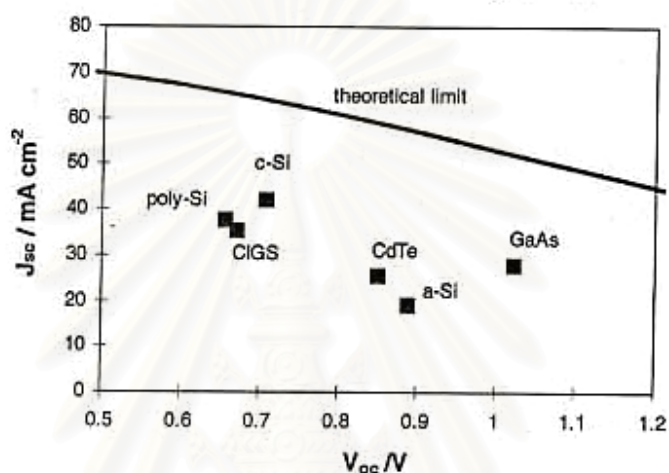


Figure 3.9 Plot of J_{sc} against V_{oc} for the cells listed in Table 3.1. Materials with high V_{oc} tend to have lower J_{sc} . This is due to the band gap of the semiconductor material. The grey line shows the relationship expected in the theoretical limit.

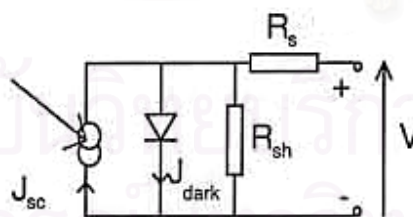


Figure 3.10 Equivalent circuit including series and shunt resistances.

The series resistance arises from the resistance of the cell material to current flow, particularly through the front surface to the contacts, and from resistive contacts. Series resistance is a particular problem at high current densities, for instance under concentrated light.

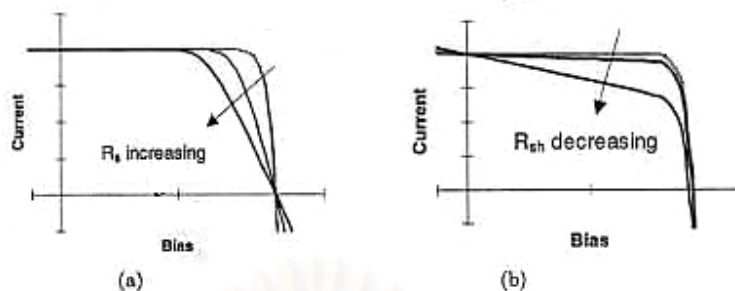


Figure 3.11 Effect of (a) increasing series and (b) reducing parallel resistances. In each case the outer curve has $R_s = 0$ and $R_{sh} = \infty$. In each case the effect of the resistance is to reduce the area of the maximum power rectangle compared to $J_{sc} \times V_{oc}$

The parallel or shunt resistance arises from leakage of current through the cell, around the edges of the device and between contacts of different polarity. It is a problem in poorly rectifying devices.

Series and parallel resistances reduce the fill factor as shown in Fig. 3.11. For an efficient cell we want R_s to be as small and R_{sh} to be as large as possible.

When parasitic resistances are included, the diode equation becomes

$$J = J_{sc} - J_0 \left(e^{q(V + JAR_s)/kT} - 1 \right) - \frac{V + JAR_s}{R_{sh}}. \quad (3.11)$$

The ‘ideal’ diode behavior of Eq. 3.5 is seldom seen. It is common for the dark current to depend more weakly on bias. The actual dependence on V is quantified by an ideality factor, m and the current-voltage characteristic given by the non-ideal diode equation, m typically lies between 1 and 2.

$$J = J_{sc} - J_0 \left(e^{qV/mk_B T} - 1 \right). \quad (3.12)$$

3.2. Dye Sensitized Solar Cell

This section contains excerpts from a book by Peter Würfel [2005]

A very good example of the solar cell structure required, with membranes for electron on side and for holes on the other side, is the electrochemical dye solar cell, as shown in Figure 3.12. The “semiconductor” in which the absorption of photons produces electron-hole pairs is a dye layer. Since the electrons and holes in the dye layer have very small motilities, this layer must be very thin in order for the charge carriers to reach the membranes within their lifetimes.

The dye is applied as a monomolecular layer to a good electron conductor in the form of TiO_2 . As Figure 3.12 illustrates, the electrons in the dye reach the conduction band of the TiO_2 without difficulty. However, due to the large band gap of more than 3 eV of TiO_2 , the holes present in the dye encounter a high barrier for the transition to the valence band of the TiO_2 .

On the other hand, the thin, only monomolecular dye layer required for efficient charge transfer has the disadvantage that the absorption of photons in one layer is very poor, since their penetration depth $1/\alpha$ into the dye is much larger than the thickness of the dye layer. In order to compensate for this disadvantage, the TiO_2 layer is therefore composed of particles, only a few nm in size, in a porous structure. All TiO_2 particles are coated with the dye on their free surfaces, so that complete absorption of the photons is achieved with the many dye layers encountered by the photons.

The porous structure, however, greatly complicates the contact between the dye and a p-n type hole membrane, through which the holes can flow outwards. This problem is solved with the use of an electrolyte that penetrates into all the pores. The iodine ions of an iodine redox system (I/I_3) provide for charge transport. The energy of an electron in I differs only very slightly from the energy of an electron in the ground state of the dye, so that the flow of holes from the dye to the electrolyte is unproblematic. The flow

of the excited electrons from the dye into the electrolyte is, however, prevented since the electrolyte has no states at the energy of the excited electrons.

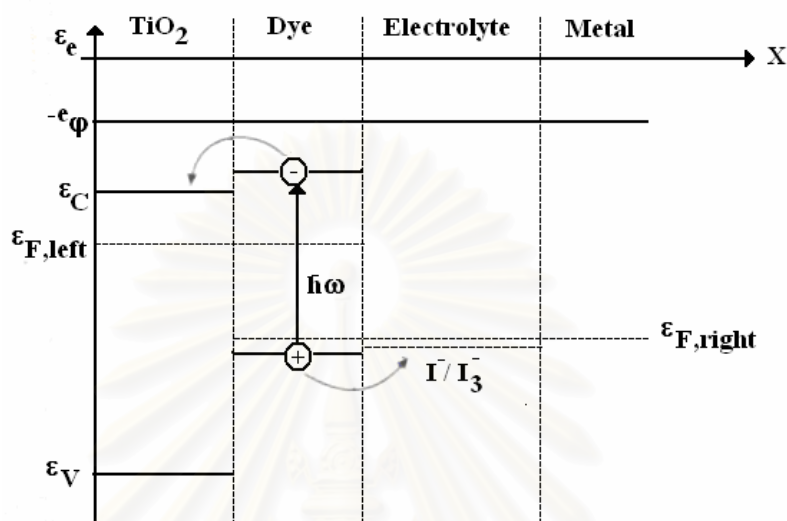


Figure 3.12 Dye solar cell in which the electron-hole pairs are produced in a ruthenium bipyridil dye. The electrons flow outwards towards the left through the n-conductor TiO_2 and the holes towards the right through the iodine ions with which the acetonitrile electrolyte is doped.

At first glance, this electrochemical cell would appear almost ideally to fulfil the requirements for the selective transport of electrons towards the left in the TiO_2 and of holes towards the right in the electrolyte. Besides direct recombination via the direct transition of an electron from its excited state in the dye to its ground state, there is also recombination via an indirect path which we can regard as an internal shunt. Excited electrons which flow to the conduction band of the TiO_2 can also reach the ground state of the dye via surface states of the TiO_2 particles, either directly or after a transition to the redox system. This back-reaction of the electrons is facilitated by the large surface area of the TiO_2 , which is, however, required in order to combine sufficient absorption with the poor transport properties of the dye. It is therefore not certain whether the dye solar cell represents a solar cell suitable for practical application. The absorption of the dye needs improvement by extending it over a greater spectral region. Problems remaining to be clarified include its stability over a period of 20 years with respect to decomposition

reaction and the possibility of the electrolyte leaking out or drying out. A solid state hole conductor would be preferable, but a way has to be found to fill it into all these tiny pores.

3.3. Titanium Dioxide

3.3.1. Physical and Chemical Properties (*Othmer, 1991 and Fujishima et al., 1999*)

Titanium dioxide may take on any of the following three crystal structures: anatase, which tends to be more stable at low temperature; brookite, which is usually found only in minerals; and rutile, which tends to be more stable at higher temperatures and thus is sometimes found in igneous rock.

Anatase generally shows a higher photocatalytic activity than the other types of titanium dioxide. Comparison of some physical properties of anatase, brookite and rutile is listed in Table 3.2.

Although anatase and rutile are both tetragonal, they do not have the same crystal structures. Anatase exists in near-regular octahedral structure and rutile forms slender prismatic crystal. Rutile is the thermally stable form and is one of the two most important ores of titanium.

The three forms of titanium (IV) oxide have been prepared in laboratories but only rutile, the thermally stable form, has been obtained in the form of transparent large single crystal. The transformation from anatase to rutile is accompanied by the evolution of ca. 12.6 kJ/mol (3.01 kcal/mol), but the rate of transformation is greatly affected by temperature the presence of other substances, which may either catalyze or inhibit the reaction. The lowest temperature at which transformation from anatase to rutile takes place at a measurable rate is around 700°C, but this is not a transition temperature. The change is not reversible since ΔG for the change from anatase to rutile is always negative.

Table 3.2 Comparison of rutile, brookite and anatase. (Othmer, 1991 and Fujishima et al., 1999).

Properties	Anatase	Brookite	Rutile
Crystal structure	Tetragonal	Orthorhombic	Tetragonal
Optical	Uniaxial, negative	Biaxial, positive	Uniaxial, negative
Density, g/cm ³	3.9	4.0	4.23
Hardness, Mohs scale	5 ^{1/2} – 6	5 ^{1/2} – 6	7 – 7 ^{1/2}
Unit cell	D _{4h} ¹⁹ .4TiO ₂	D _{2h} ¹⁵ .8TiO ₂	D _{4h} ¹² .3TiO ₂
Dimension, nm			
a	0.3758	0.9166	0.4584
b	-	0.5436	-
c	0.9514	0.5135	2.953
Refractive index	2.52	-	2.52
Permittivity	31	-	114
Melting point	changes to rutile at high temperature	-	1858°C

Brookite has been produced by heating amorphous titanium (IV) oxide, which is prepared from an alkyl titanate or sodium titanate, with sodium or potassium hydroxide in an autoclave at 200 to 600 °C for several days. The important commercial forms of titanium (IV) oxide are anatase and rutile, and they can readily be distinguished by X-ray diffractometry.

Since both anatase and rutile are tetragonal, both of them are anisotropic, and their physical properties, e.g., refractive index, vary according to the direction relative to the crystal axes. In most applications of these substances, the distinction between

crystallographic direction is lost because of the random orientation of large numbers of small particles, and only average values of the properties are significant.

Measurement of physical properties, in which the crystallographic directions are taken into account, may be made for both natural and synthetic rutile, natural anatase crystals, and natural brookite crystals. Measurements of the refractive index of titanium (IV) oxide must be made by using a crystal that is suitably orientated with respect to the crystallographic axis as a prism in a spectrometer. Crystals of suitable size of all three modifications occur naturally and have been studied. However, rutile is the only form that can be obtained in large artificial crystals from melts. The refractive index of rutile is 2.75. The dielectric constant of rutile varies with direction in the crystal and any variation from the stoichiometric formula, TiO_2 . An average value for rutile in powder form is 114. The dielectric constant of anatase powder is 48.

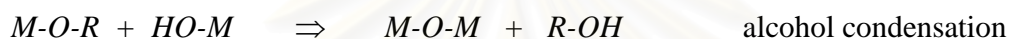
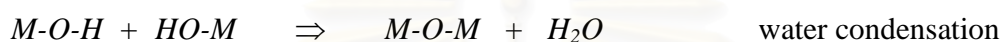
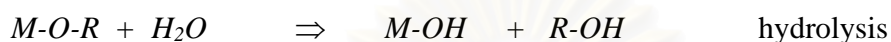
3.3.2 Applications of titanium dioxide

Titanium dioxide is one of the most basic materials in our daily life. Titanium dioxide has been used in paints, plastics, paper, inks, fibers, cosmetics, sunscreens and foodstuffs.

Naturally, the type of titanium dioxide that is used as a pigment is different from that used as a photocatalyst. Various applications in which research and development activities involving titanium dioxide have been investigated, such as fog-proof, anti-bacterial, anti-viral, fungicidal, anti-soiling, self-cleaning, deodorizing, air purification, anti-cancer, water treatment and water purification.

3.4. Sol-gel Method (*Fu et al., 1996 and Su et al., 2004*)

Sol-gel process occurs in liquid solution of organometallic precursors such as tetraethyl orthosilicate, zirconium propoxide and titanium isopropoxide, which, by means of hydrolysis and condensation reaction, lead to the formation of sol.



A typical example of a sol-gel method is the addition of metal alkoxides to water. The alkoxides are hydrolyzed, giving the oxide as a colloidal product.

The sol is made of solid particles of a diameter of few hundred nanometers suspending in a liquid phase. After that, the particles condense into gel, in which solid macromolecules are immersed in a liquid phase. Drying the gel at low temperature (25-100°C), produces porous solid matrices or xerogels. To obtain a final product, the gel is heated. This heat treatment serves several purposes, i.e., to remove solvent, to decompose anions such as alkoxides or carbonates to give oxides, to rearrange of the structure of the solid, and to allow crystallization to occur.

Using the sol-gel method, one can easily control a stoichiometry of solid solution and a homogeneous distribution of nanoparticles and metal oxides. In addition, the advantages are that the metal oxides are prepared easily at room temperature and high purity can be obtained.

CHAPTER IV

EXPERIMENTAL

The organization of this chapter is as follows: preparation of TiO₂ sol and modified TiO₂ sols, components of dye-sensitized solar cell, fabrication of dye-sensitized solar cell, and characterization techniques employed in this study.

4.1 Preparation of TiO₂ sol and modified TiO₂ sols

TiO₂ was synthesized via a sol-gel method. TiO₂ constituted an electrode layer of a DSSC in the study. A TiO₂ electrode layer was then modified by addition of vanadium chloride, scandium chloride and tetracyanoquinodimethane (TCNQ) to the sol.

4.1.1 Preparation of TiO₂ sol

TiO₂ was synthesized via a sol-gel method. First, one mixed 28 ml of 70% nitric acid and 900 ml of deionized water. Titanium (IV) isopropoxide in the amount of 75.20 ml was added slowly to the solution while being stirred continuously. The mixture was stirred for 3-4 days until clean sol was obtained. Next, the clean sol underwent dialysis in a cellulose membrane. The water used for dialysis was changed daily until a pH 3.5 was obtained. The resulting TiO₂ sol was kept in a refrigerator until needed.

4.1.2 Modification of TiO₂ sol

In this research, we added other compounds to modify TiO₂ layer in dye-sensitized solar cell in an attempt to improve efficiency of the cell.

The compounds chosen for this study were vanadium chloride (VCl_3) and scandium chloride ($ScCl_3$). Tetracyanoquinodimethane (TCNQ) was also chosen as a modifier. Scandium or vanadium compounds were added to a TiO_2 sol at concentrations of 2%, 5% and 9% (w/w). We assumed that one liter of TiO_2 contained 15 grams of TiO_2 particles. Meanwhile, the concentrations of TCNQ that were added to a TiO_2 sol were 2%, 5%, 9%, 12%, 15%, and 19% (w/w).

4.1.2.1 Adding vanadium chloride

To obtain 2%, 5%, and 9% (w/w) of VCl_3 in TiO_2 sol, we mixed 0.010 g, 0.025 g, and 0.045 g of VCl_3 with TiO_2 sol with the volumes of 32.70 ml, 31.70 ml, and 30.30 ml respectively. The solution was stirred until homogeneity was obtained. The final solution was reddish brown.

4.1.2.2 Adding scandium chloride

To obtain 2%, 5%, and 9% (w/w) of $ScCl_3$ in TiO_2 sol, we mixed 0.010 g, 0.025 g, and 0.045 g of $ScCl_3$ with TiO_2 sol with the volumes of 32.70 ml, 31.70 ml, and 30.30 ml respectively. The solution was stirred until homogeneity was obtained. The final solution was transparent.

4.1.2.3 Adding tetracyanoquinodimethane (TCNQ)

TCNQ was added to TiO_2 sol at concentrations of 2%, 5%, 9%, 12%, 15%, and 19% (w/w). First, TCNQ was grounded in order to be easily suspended in the sol. Then, 0.010 g, 0.025 g, 0.045 g, 0.060 g, 0.075 g, and 0.095 g of grounded TCNQ were added to 32.70 ml, 31.70 ml, 30.30 ml, 29.30 ml, 28.30 ml, and 27.00 ml of TiO_2 sol so as to obtain suspensions of 2%, 5%, 9%, 12%, 15%, and 19% (w/w) TCNQ in TiO_2 sol.

4.2 Preparation of dye-sensitized solar cell components and the fabrication procedure

This section discusses preparation of components in dye-sensitized solar cell (DSSC) and the fabrication procedure for DSSC. The components of DSSC are mainly considered of conducting glass, counter electrode, electrolyte, TiO₂ electrode, dye, and sealing material.

4.2.1 Dye

In our research, we used Cis-di(thiocyanate)bis(2,2'-bipyridine-4,4'-dicarboxylate)ruthenium(II) or N3 (R535) dye, which is widely used in dye-sensitized solar cell. To prepare the dye solution, 20 mg of N3 dye was dissolved in 100 ml of ethanol and the mixture was stirred until a homogeneous solution was obtained. The resulting product is a solution of 0.3 mM N3 dye in ethanol.

4.2.2 Electrolyte

In this study, two types of electrolytes, namely, electrolyte I and electrolyte II were investigated. Preparation of the two electrolytes is presented in this section.

4.2.2.1 Electrolyte I

Electrolyte I consisted of 0.6 M dimethylpropylimidazolium iodide (DMP II), 0.1 M lithium iodine (LiI), 0.05 M iodine (I₂), and 0.5 M 4-tert-butylpyridine (TBP) in acetonitrile. The recipe was obtained from previous work done by Ngamsinlapasathian and coworkers [2004]. To prepare electrolyte I, we mixed 4.79 g of DMP II, 0.40 g of LiI, 0.38 g of I₂, and 2.20 ml of TBP in 30 ml of acetonitrile.

4.2.2.2 Electrolyte II

Electrolyte II consisted of 0.5 M lithium iodine (LiI), 0.05 M iodide (I_2), and 0.5 M 4-tert-butylpyridine (TBP) in acetonitrile. The recipe was obtained from previous work done by Huang and coworkers [2005]. To prepare electrolyte II, we mixed 2.00 g of LiI, 0.38 g of I_2 , and 2.20 ml of TBP in 30 ml of acetonitrile.

4.2.3 Platinum counter electrode

The counter electrode for the DSSC is platinum coated on conducting glass. The conducting glass is transparent conducting oxide coated glass, which is tin oxide (SnO_2) coated electrically conducting glass. The glass was purchased from Asahi Glass (Japan) under a commercial name DU type. There are two ways in preparation of platinum counter electrode. The first method is sputtering and the second is coating with platinum precursor, followed by heating. Sputtering technique was chosen for this study because thickness of platinum layer can be controlled easily.

To prepare a platinum counter electrode, we first cut a conducting glass to a rectangular piece that was 1.0 cm wide and 1.5 cm long. Masking tape was placed on one side of the glass as seen in Figure 4.1. The surface of the glass was cleaned with methanol.

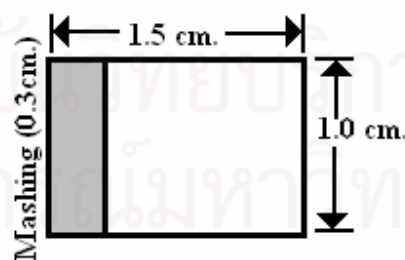


Figure 4.1 Schematic diagram of a platinum counter electrode

Then, platinum was sputtering on the conducting glass for four minutes. After sputtering, masking tape was removed.

4.2.4 TiO₂ anode electrode

Anode electrode consisted of TiO₂ film on a conducting glass. To prepare the electrode, we first cut a conducting glass into a rectangular piece that was 1.0 cm wide and 1.5 cm long. The glass was cleaned with methanol. Then the glass was masked with aluminum foil of the same size. A 0.5×0.5 cm square was cut out of the aluminum foil (as seen in Figure 4.2). The cut out was located closer to one side of the foil than the other.

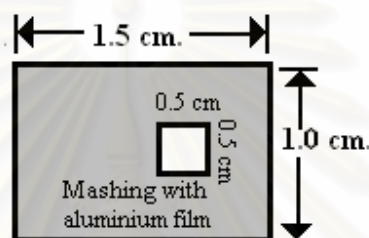


Figure 4.2 Show anode electrode before sprayed

After masking, TiO₂ was coated on the glass using ultrasonic spray coater. The spraying liquid (e.g., TiO₂ sol) was placed in a syringe pump, which fed the liquid at a rate 1 ml/min to an ultrasonic nozzle. The masked glass was placed on a moving platform, which went back and forth under the nozzle. The speed of a moving stage was at level 1 out of 4. The power of an ultrasonic nozzle, provided by a frequency generator until, was 3.5 watts.

The number of coats of TiO₂ was varied. We chose 30, 50, 70, 100, 150, 180, and 220 coats of TiO₂ for this study. After a few coats, TiO₂ film was dried by a blow dryer. The numbers of coats before each drying are listed in Table 4.1. Note that the number of coats before each drying became larger as the number of coats increased.

After the desired number of coats of TiO₂ was applied, the coated glass was left to cool down at room temperature for two hours. Then the coated glass was fired in a furnace at a temperature ranging from 200 °C to 500 °C for two hours. Next, the glass was immersed in a solution of 0.3 mM N3 dye in ethanol for 10 hours in the dark.

Table 4.1 Number of coats of TiO₂ applied before each drying

number of coats		
2 coats	dry with blow dryer	
2 coats	dry with blow dryer	
2 coats	dry with blow dryer	
2 coats	dry with blow dryer	
2 coats	dry with blow dryer	
4 coats	dry with blow dryer	
4 coats	dry with blow dryer	
4 coats	dry with blow dryer	
4 coats	dry with blow dryer	
4 coats	dry with blow dryer	30 coats
6 coats	dry with blow dryer	
6 coats	dry with blow dryer	
6 coats	dry with blow dryer	50 coats
6 coats	dry with blow dryer	
6 coats	dry with blow dryer	
8 coats	dry with blow dryer	70 coats
8 coats	dry with blow dryer	
8 coats	dry with blow dryer	
8 coats	dry with blow dryer	
8 coats	dry with blow dryer	100 coats
10 coats	dry with blow dryer	
10 coats	dry with blow dryer	
10 coats	dry with blow dryer	
10 coats	dry with blow dryer	
10 coats	dry with blow dryer	150 coats
10 coats	dry with blow dryer	
10 coats	dry with blow dryer	
10 coats	dry with blow dryer	180 coats
10 coats	dry with blow dryer	
10 coats	dry with blow dryer	
10 coats	dry with blow dryer	
10 coats		220 coats

4.2.5 Fabrication of dye-sensitized solar cell assembly

Fabrication of dye-sensitized solar cell assembly started with cutting two strips of a sealing material that were 0.15 cm wide and 1.2 cm long. The strips were attached to the top and bottom sides of an anode electrode (see Figure 4.3a). Then a platinum counter electrode was placed on top of the anode electrode so that the conducting side of the counter electrode was on top of the TiO₂ film. The two glass plates were offset, allowing the edges of each plates to be exposed (see Figure 4.3b). The cell was sealed by heating the sealing material with a blow dryer.

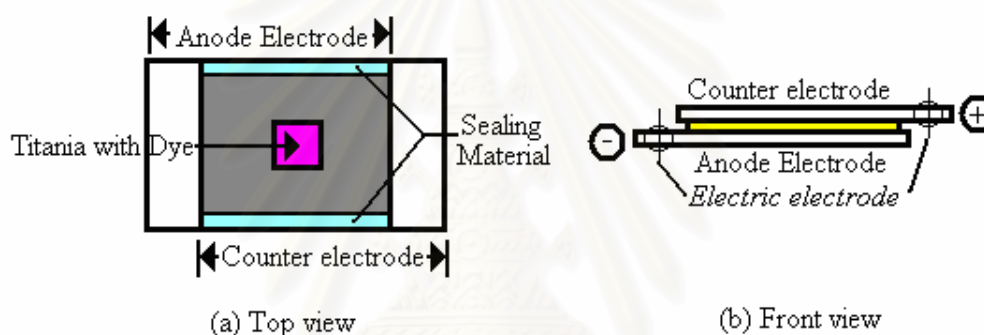


Figure 4.3 Dye-sensitized solar cell assembly before electrolyte injection

After the anode and the counter electrode were attached together by the sealing material, electrolyte solution was injected between the two glass plates. Figure 4.4 displays an arrangement of various layers within a DSSC assembly, which is ready for testing.

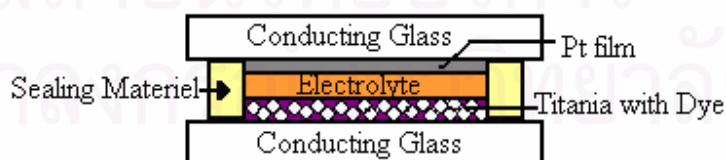


Figure 4.4 Arrangement of various layers within dye-sensitized solar cell assembly

4.3. Physical and Electrochemical Characterization

In order to determine physical and electrochemical properties of TiO₂ and DSSC, various characterization techniques were employed. Such techniques are discussed in this section.

4.3.1 X-ray diffractometry (XRD)

XRD was performed to determine crystal phase and crystallite size of TiO₂. The characterization was conducted using a SIEMENS D5000 X-ray diffractometer with Cu K_α radiation ($\lambda = 1.54439 \text{ \AA}$) with Ni filter. The spectra were scanned at a rate of $0.04^\circ \text{ min}^{-1}$ in the 2θ range of $20\text{-}80^\circ$.

4.3.2 Nitrogen physisorption

Specific surface area of TiO₂ was measured through nitrogen gas adsorption in a continuous flow method at liquid nitrogen temperature. A mixture of nitrogen and helium was employed as the carrier gas using Micromeritics ChemiSorb 2750 Pulse Chemisorption System instrument. TiO₂ powders that under went the same heating routine were used in place of TiO₂ films. The sample was thermally treated at 200°C for one hour before measurement.

4.3.3 Fourier transform infrared spectroscopy (FT-IR)

FT-IR was employed to detect organic compounds on TiO₂ surface. Prior to each measurement, the sample was mixed with KBr at a ratio of sample to KBr of 1:100 and was pressed to form a thin wafer. The equipment used was a Nicolet impact 400. IR spectra were recorded from an accumulation of 32 scans in $4000\text{-}400 \text{ cm}^{-1}$ range with a resolution of 4 cm^{-1} .

4.3.4 Thermo gravimetric Analysis (TGA)

TGA was employed to determine the amount of organic compounds remained in TiO₂ film. The equipment used was SDT analyzer model Q600. The TGA spectra were recorded from a heating rate 10 °C/minute in 33 – 600 °C. The Alumina cup was employed.

4.3.5 Current-Voltage Tester (I-V Tester)

The electrochemical properties of dye-sensitized solar cell were determined by I-V tester Current–voltage measurements were performed using white light source under air mass (AM) 1.5G conditions. One could determine current density, open circuit voltage, cell resistance, and fill factor. These information were then converted to efficiency of the solar cell. An area of our solar cell was 0.25 cm² (0.5 cm×0.5 cm). The equipment used was MVSystems Inc., Xenon short ARC (Osram XBO 1000 W/HS).

CHAPTER V

RESULTS AND DISCUSSION

The chapter are divide into four parts, namely, effect of type of electrolyte, effect of thickness of TiO₂ electrode layer, effect of temperature for sintering TiO₂ and effect of modification of TiO₂ layer on the performance of dye-sensitized solar cell.

5.1 Effect of type of electrolyte

The effect of type of electrolyte on efficiency of our dye-sensitized solar cell was investigated. Normally, it is difficult to predict what electrolyte is best for DSSC because it depends on electrochemical interaction among dye, TiO₂, and electrolyte. In our research, we compared two electrolytes in terms of efficiency of the DSSC. Electrolyte I was composed of with 0.6 M dimethylpropylimidazolium iodide (DMPII), 0.1 M lithium iodide (LiI), 0.05 M iodine (I₂) and 0.5 M 4-tert-butylpyridine (TBP) in acetonitrile (CH₃CN). Electrolyte II was composed of 0.5 M LiI, 0.05 M I₂ and 0.5 M TBP in acetonitrile. The conditions, under which the DSSC was prepared, was 180 coats of TiO₂, a sintering temperature of 400 °C, and an area of cell of 0.25 cm². The results from the measurements by an I-V tester are show in table 5.1.

Table 5.1 Electrochemical properties of DSSC with different electrolyte

Electrolyte	V _{OC} (Volt)	J _{SC} (mA/cm ²)	Fill Factor	Efficiency (%)
Electrolyte I	0.68	1.98	0.78	1.05
Electrolyte II	0.67	2.45	0.72	1.19

From Table 5.1, the open-circuit voltage (V_{OC}) of the two electrolytes were similar but the short-circuit current density (J_{SC}) of electrolyte II was significantly higher than that of electrolyte I. Therefore, the efficiency of a DSSC with electrolyte II was greater than that with Electrolyte I. I-V curves of both electrolytes were shown below.

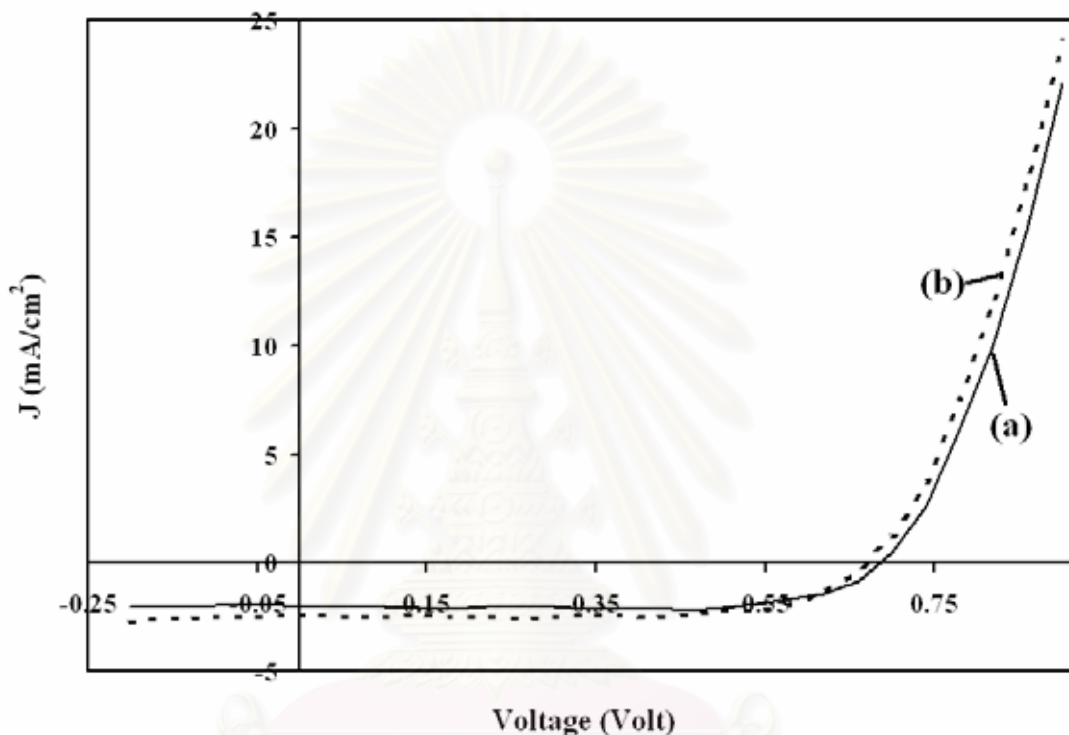


Figure 5.1 I-V curves of DSSC with (a) Electrolyte I and (b) Electrolyte II.

The difference between Electrolyte I and II was that Electrolyte I contained 0.6 M DMPII and 0.1 M LiI while Electrolyte II contained 0.5 M LiI. Therefore, the presence of DMP II and Li^+ ion may cause the different efficiency of DSSC. Redmond and coworkers (1993) suggested that the lower V_{oc} for LiI was caused by a positive shift of the conduction band edge level of the TiO_2 electrode due to intercalation or adsorption of Li cations. Hara and coworkers (2004) stated that combination of Li and DMPII cations improved the J_{sc} , although the detailed mechanism is not clear. On other hand, Kawano (2003) reported that fast charge transport of an I^-/I_3^- redox couple in electrolyte was attributed to the contribution of the exchange reaction between I^- and I_3^- , and the

contribution to the total charge transport process dominated when concentration of the redox couple was high, and $[I^-]$ and $[I_2]$ were similar. The concentrations of I^- and I_2 in Electrolyte II (0.5 M and 0.05 M) were closer when compared with Electrolyte I (0.7 M and 0.05 M). In addition, Kuang and coworkers (2006) reported that the addition of Li^+ to a nonvolatile liquid electrolyte gave rise to a significant increase in the photocurrent density, with only a small decrease in the open-circuit voltage. For Electrolyte II there is small drop in the open-circuit voltage accompanied by a large increase in the photocurrent density upon the addition of Li^+ compared with Electrolyte I. The V_{oc} was reduced by the surface adsorption of Li^+ , resulting in a positive shift of the conduction band of TiO_2 and consequently caused a drop in the open-circuit voltage of the cell. But the adsorption of a high concentration of Li^+ on the TiO_2 surface gave a globally positive charge to the surface, increasing the local concentration of iodide and hence increasing the dye regeneration rate. And the high concentration of ions was held on the dye molecules and thus caused an increasingly strong “charge screening” effect. This effect would reduce the charge recombination rate. And then the charge screening and globally positive charge to the surface would result in efficiency of DSSC with Electrolyte II being higher than that with Electrolyte I.

5.2 Effect of Sintering Temperature for TiO_2 Electrode

TiO_2 sol was prepared via sol-gel method and was used to make anode electrode. One can easily control physical properties of TiO_2 particles via sintering temperature and sintering time. Sintering temperature of TiO_2 could affect specific surface area, crystal size, pore volume and pore size. These properties had influence on efficiency of dye-sensitized solar cell. In this study, we varied the sintering temperature to be 200 °C, 300 °C, 400 °C and 500 °C. Since TiO_2 thin film was not suitable for several characterization techniques, we employed TiO_2 powder that under went the same treatment as a surrogate for characterization purpose.

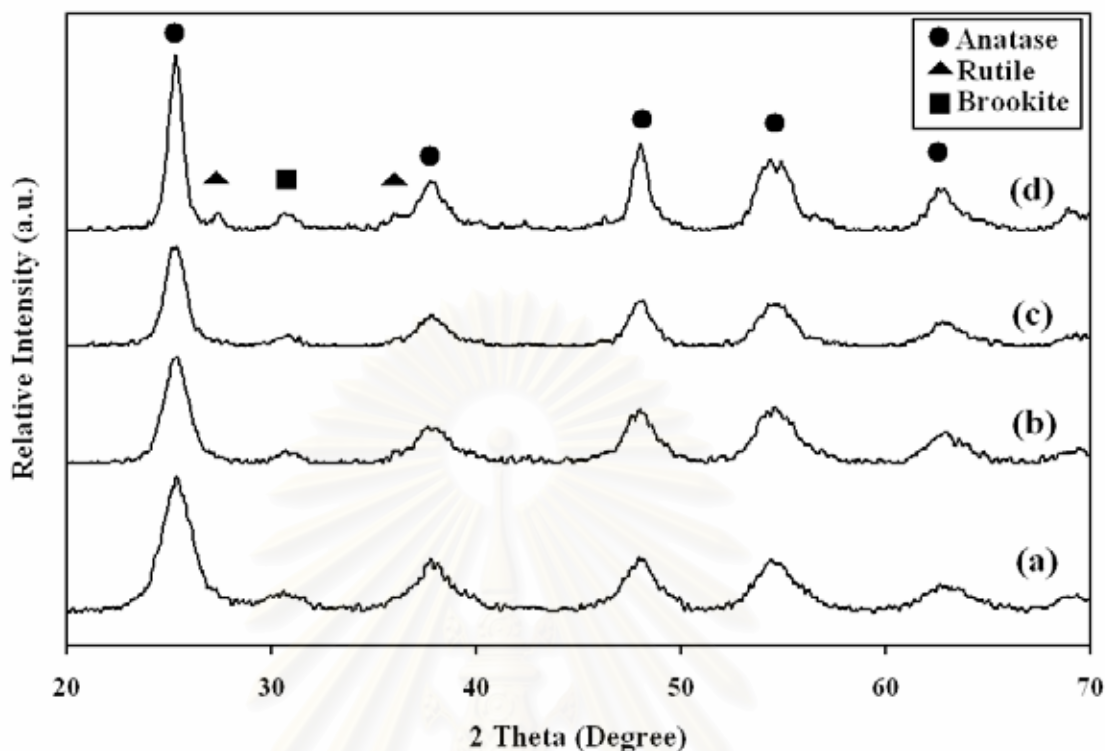


Figure 5.2 Results from XRD for TiO_2 powders that were fired at, (a) 200 °C, (b) 300 °C, (c) 400 °C, and (d) 500 °C

Figure 5.2 indicated that the major phase of TiO_2 powder was anatase with a small amount of brookite for all samples. Rutile was detected for TiO_2 powder that was fired at 500 °C. Next, we determined Specific surface area and average pore size of TiO_2 powders from nitrogen adsorption technique. The results are presented in Table 5.2.

Crystallite sizes of TiO_2 grew from 4.9 nm to 11.7 nm as sintering temperature was raised from 200°C to 500°C. At the same time, the Specific surface area of TiO_2 decreased from 234 m^2/g to 97 m^2/g and the average pore size grew from 40 Å to 69 Å. Huang and coworkers [2006] reported that different parameters such as pore diameter, particle size, and specific surface area of TiO_2 played important roles on the performance of the solar cell. For this study, the solar cell consisted of 180 coats of TiO_2 as anode electrode, Electrolyte II as an electrolyte, and the temperature used for sintering ranging

from 200°C to 500°C, Electrochemical properties of the cells were determined and the results are listed in Table 5.2.

Table 5.2 Physical properties of TiO₂ powders as obtained from XRD and nitrogen adsorption

Temperature for sintering TiO ₂ (°C)	Crystal Size (nm) from XRD	BET Surface Area (m ² /g)	Pore Size (Å)
200	4.9	234	40
300	5.2	192	51
400	7.0	149	61
500	11.7	96	69

Table 5.3 Electrochemical properties of DSSC of which TiO₂ electrode was fired at various temperatures.

Temperature (°C)	V _{OC} (Volt)	J _{SC} (mA/cm ²)	Fill Factor	Efficiency (%)
200	0.52	1.20	0.35	0.22
300	0.64	1.83	0.57	0.67
400	0.67	2.45	0.72	1.19
500	0.67	3.52	1.74	1.60

In order to visualize the effect of sintering temperature on efficiency of DSSC, a plot of cell efficiency vs. sintering temperature was made (as seen in Figure 5.3).

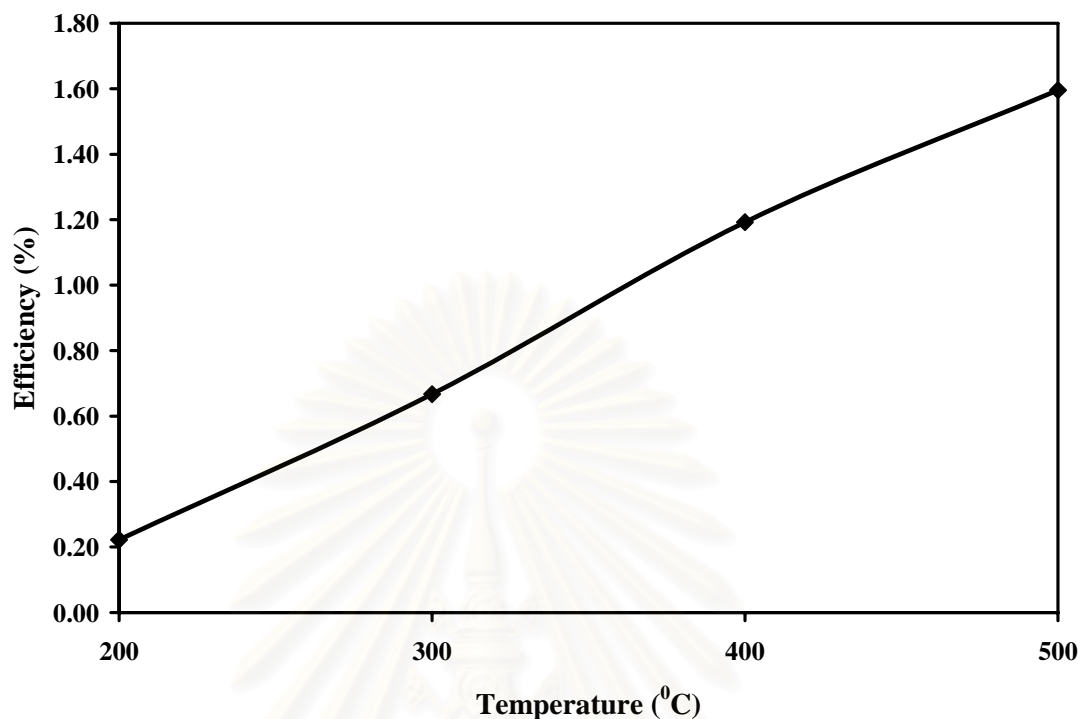


Figure 5.3 Efficiency of DSSC as a function of sintering temperature of DSSC

From Table 5.3, the open-circuit voltage (V_{oc}) increased from 0.52 V to 0.67 V when sintering temperature was increased from 200 °C to 400 °C but remained steady when temperature was increased from 400 °C to 500 °C. On the other hand, the short-circuit current density increased steadily from 1.20 mA/cm² to 3.53 mA/cm² when sintering temperature was increased from 200 °C to 500 °C. The fill factor (FF) of the cell increased from 0.35 to 0.72 when sintering temperature was increased from 200 °C to 400 °C but dropped to 0.66 at 500 °C. From Figure 5.3, the efficiency of our cells increased from 0.22 % to 1.60 % when sintering temperature for TiO₂ was increased from 200 °C to 500 °C. This result was in good agreement with work done by Huang and coworkers (2006). When pore diameter was too small to allow the transport of iodide/tri-iodide ionic species (I/I_3^-) within the pores of the TiO₂ films, the efficiency of cell was low. When sintering temperature of TiO₂ film was increased, the average pore size became larger (see Table 5.2). Longer pores brought sufficient space for the diffusion of the iodide/tri-iodide ionic species (I/I_3^-) into the TiO₂ matrix, leading to maximum cell efficiency for sintering temperature of 500 °C. However, we further inspected an I-V

curve of a cell, of which TiO_2 layer was fired at 500°C , because of strange behavior observed regarding V_{oc} and FF. The I-V curve was displayed in Figure 5.4.

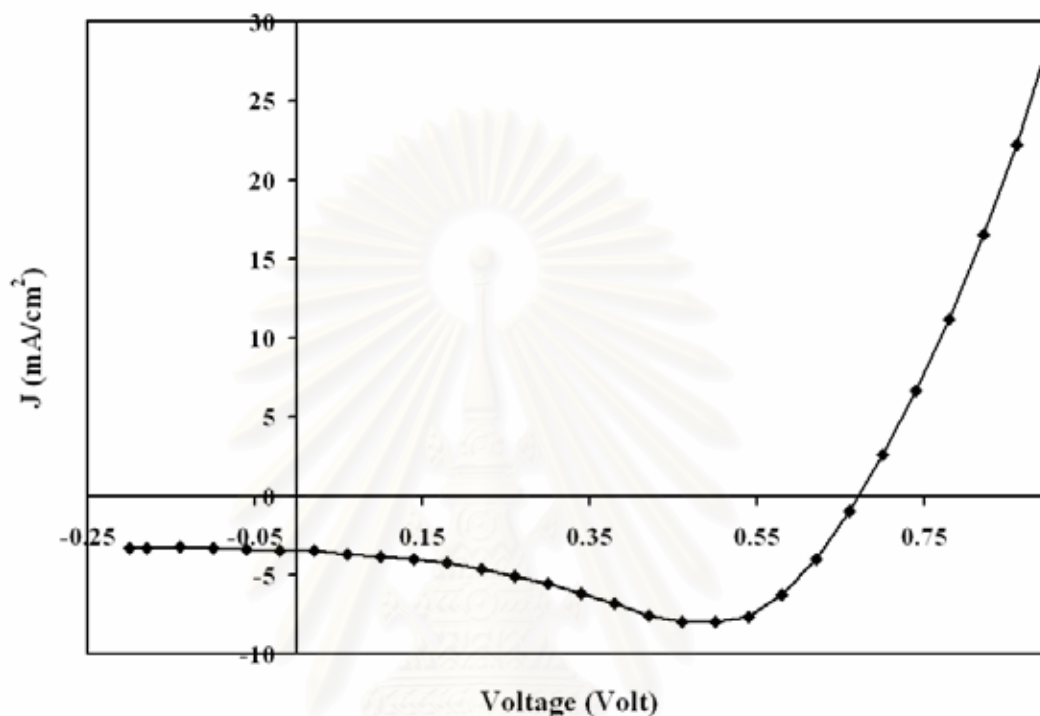


Figure 5.4 I-V curve of dye-sensitized solar cell, of which TiO_2 electrode layer was fired at 500°C .

The I-V curve in Figure 5.4 did not exhibit normal characteristics of dye-sensitized solar cell. Normally, the base line should be horizontal and be parallel with voltage axis. Since the curve was not horizontal, there was an error in the calculation of the fill factor by the program. Then the calculation for the fill factor was repeated manually and the resulting fill factor is 0.66 (instead of 1.74 obtained from the program). The manual calculation of fill factor is shown in Appendix A. In conclusion, even when a sintering temperature of 500°C produced the highest efficiency for the solar cell, 400°C may be better because of the strange behavior of an I-V curve for 500°C .

5.3 Effect of Thickness of TiO₂ Film

In this part, we varied the thickness of TiO₂ electrode layer by varying number of coats of TiO₂ that were sprayed on the substrate. The thickness of TiO₂ electrode layer played an important role on the performance of the solar cell [Huang et al., 2006]. The numbers of coats of TiO₂ for this study were 30, 50, 70, 100, 150, and 220 coats. The sintering temperature for TiO₂ was 400°C. The electrochemical properties of the solar cell are listed in Table 5.4. Figure 5.5 displays the efficiency of DSSC as a function of number of coats of TiO₂ for the electrode layer.

Table 5.4 Electrochemical properties of dye-sensitized solar cells with various thickness of TiO₂ electrode layer.

Numbers of coats of TiO ₂	V _{OC} (Volt)	J _{SC} (mA/cm ²)	Fill Factor	Efficiency (%)
30	0.54	1.68	0.67	0.61
50	0.63	1.90	0.61	0.73
70	0.57	2.96	0.65	1.08
100	0.67	2.34	0.79	1.23
150	0.70	2.47	0.75	1.30
220	0.66	2.16	0.87	1.23

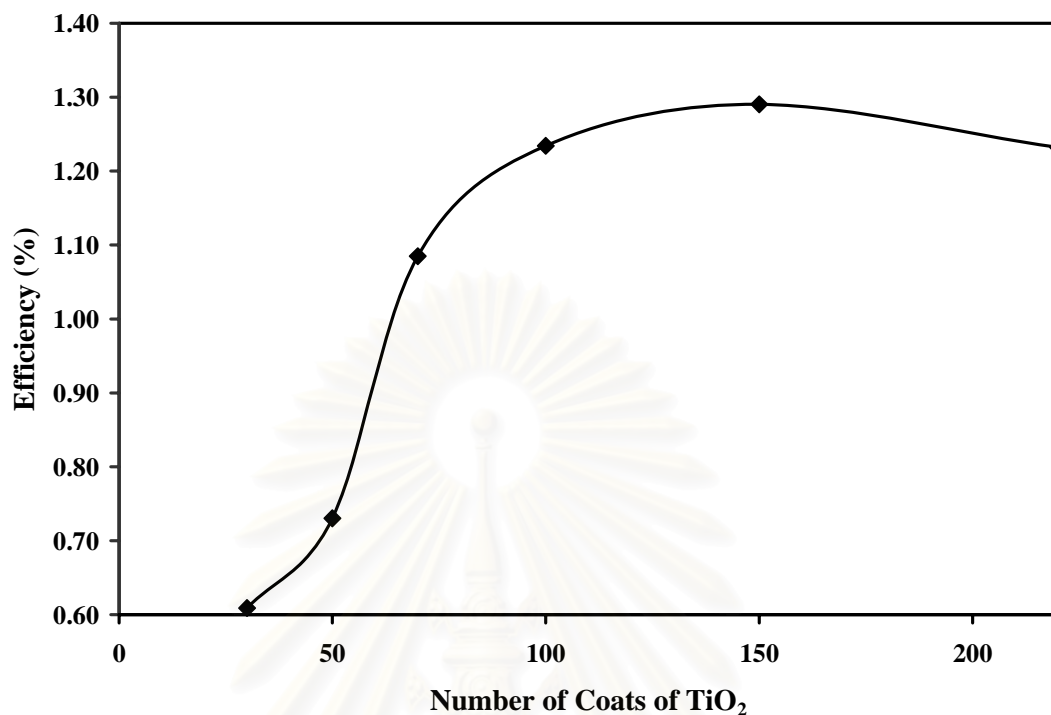


Figure 5.5 Efficiency of DSSC as a function of number of coats of TiO₂ for the electrode

From Figure 5.5, the efficiency of a DSSC increased from 0.61% to 1.30% when the number of coats of TiO₂ was increased from 30 to 150. A further increase in the number of coats of TiO₂ from 150 to 220 did not result in an increase in the efficiency of DSSC. Generally, thicker film could adsorb more dye molecules leading to an enhancement in the photocurrent of the dye-sensitized solar cell. This behavior could be explained by consideration of pore sized of TiO₂ and other molecules involved. From Table 5.2 the average pore size of TiO₂ that was fired was 6.1 nm. The size of an N3 dye molecule was 1.5 nm as reported by Fillinger and coworkers [2002]. The size of tri-iodide ion in acetonitrile was approximately 4 nm, according to Hawlicka and coworkers [1990]. Therefore, pores in TiO₂ layer were large enough for dye molecule and tri-iodide ion. Still there was diffusion space left for the redox couple. If the TiO₂ film was thicker than a certain value, it would be very difficult for the diffusion of the redox couple into the TiO₂ matrix. As a result, only a finite amount of dye molecules was reduced by iodide ions, limiting the current and the efficiency to be constant [Huang et al., 2006]. For our study, the optimum number of coats of TiO₂ was 150.

5.4 Effect of modification of TiO₂ electrode layer

5.4.1 Modification of TiO₂ electrode layer by scandium and vanadium

TiO₂ electrode layer was modified by addition of the second compounds, i.e., scandium compound, vanadium compound, and tetracyanoquinodimethane (TCNQ), to TiO₂ sol. Vanadium has one more electron in the valence shell than titanium, while scandium has one lower electron. These differences in numbers of valence electron should alter the Fermi level of titanium dioxide, leading to an improvement in electron transfer process. Figure 5.6 shows the periodic table of vanadium, titanium, and scandium and their electronic configurations.

12 Mg Magnesium		IIIB	IVB	VB	VIB	VIIB
20 Ca Calcium	21 Sc Scandium (Ar)3d ¹ 4s ²	22 Ti Titanium (Ar)3d ² 4s ²	23 V Vanadium (Ar)3d ³ 4s ²	24 Cr Chromium		

Figure 5.6 The periodic table that contains scandium, titanium and scandium.

The precursors for scandium and vanadium were chosen to be vanadium chloride and scandium chloride, respectively, because of their solubilities in TiO₂ sol. The concentrations of scandium and vanadium in the solution were 2%, 5% and 9% (w/w) in TiO₂ sol. Characterization of modified TiO₂ was performed on TiO₂ powders that contained the same amount of either scandium and vanadium and underwent the same heat treatment. The results from XRD for TiO₂ modified with scandium and vanadium are displayed in Figure 5.7 and 5.8, respectively.

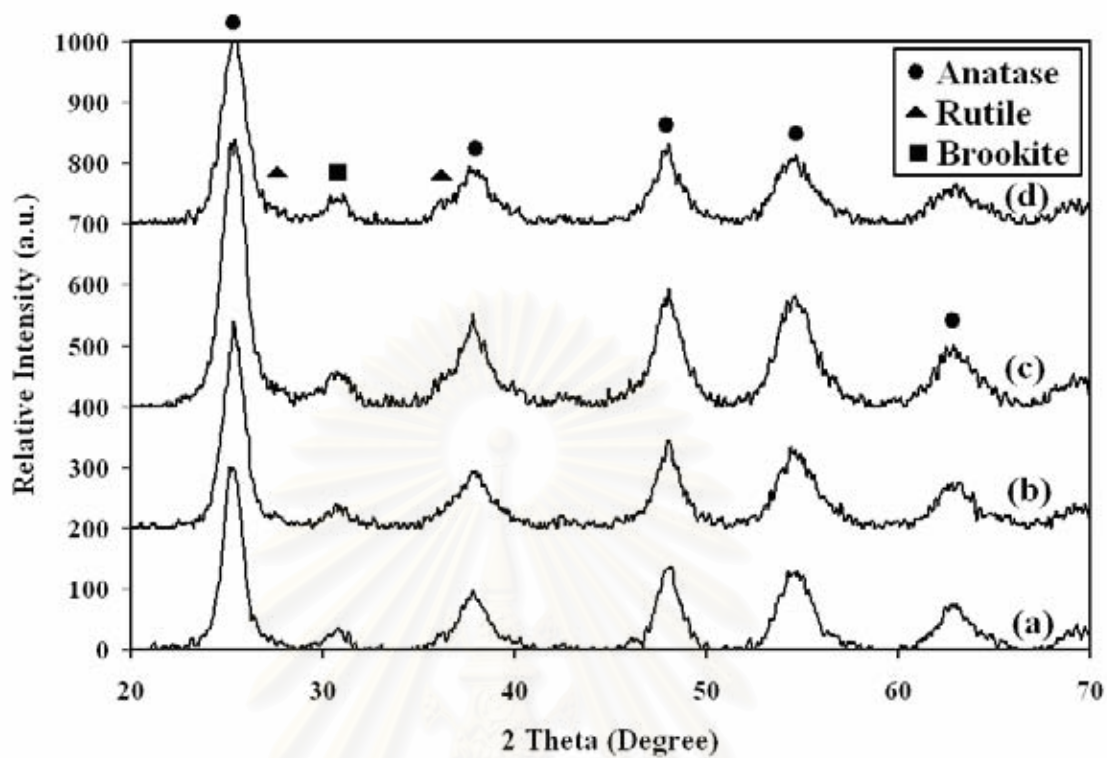


Figure 5.7 XRD results for TiO₂ powder modified with (a) 0% (w/w), (b) 2% (w/w), (c) 5% (w/w), and (d) 9% (w/w) of scandium.

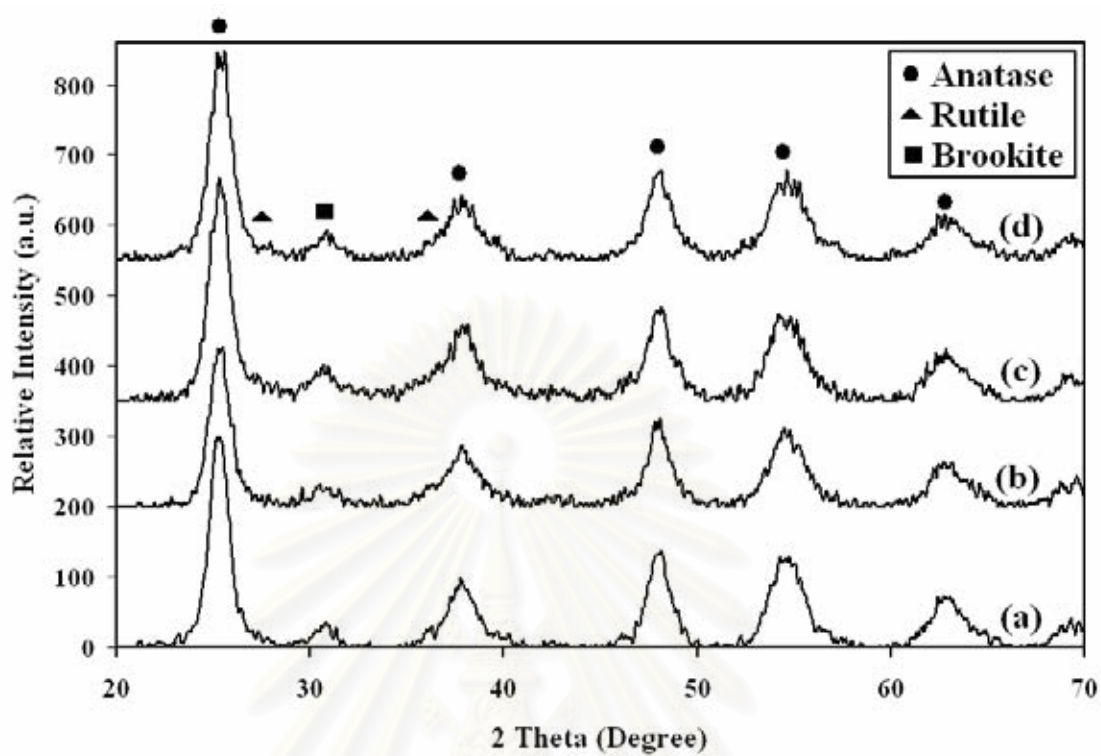


Figure 5.8 XRD results for TiO₂ powder modified with (a) 0%(w/w), (b) 2%(w/w), (c) 5%(w/w), and (d) 9%(w/w) of vanadium.

Crystal phases of TiO₂ in the samples appeared to be unaffected by the addition of scandium and vanadium. However, the average crystallite sizes of modified TiO₂ were smaller than that of pure TiO₂. Moreover, the specific surface area of pure TiO₂ powder and modified TiO₂ powders were comparable (see Table 5.5).

Table 5.5 Physical data of doped TiO₂ powders by XRD and nitrogen adsorption.

%Metal (w/w)	Crystal size (nm)	Surface area (m ² /g)
Undoped TiO ₂	7.0	146
2% Scandium	7.2	165
5% Scandium	5.7	155
9% Scandium	6.1	145
2% Vanadium	6.3	140
5% Vanadium	4.1	130
9% Vanadium	6.6	139

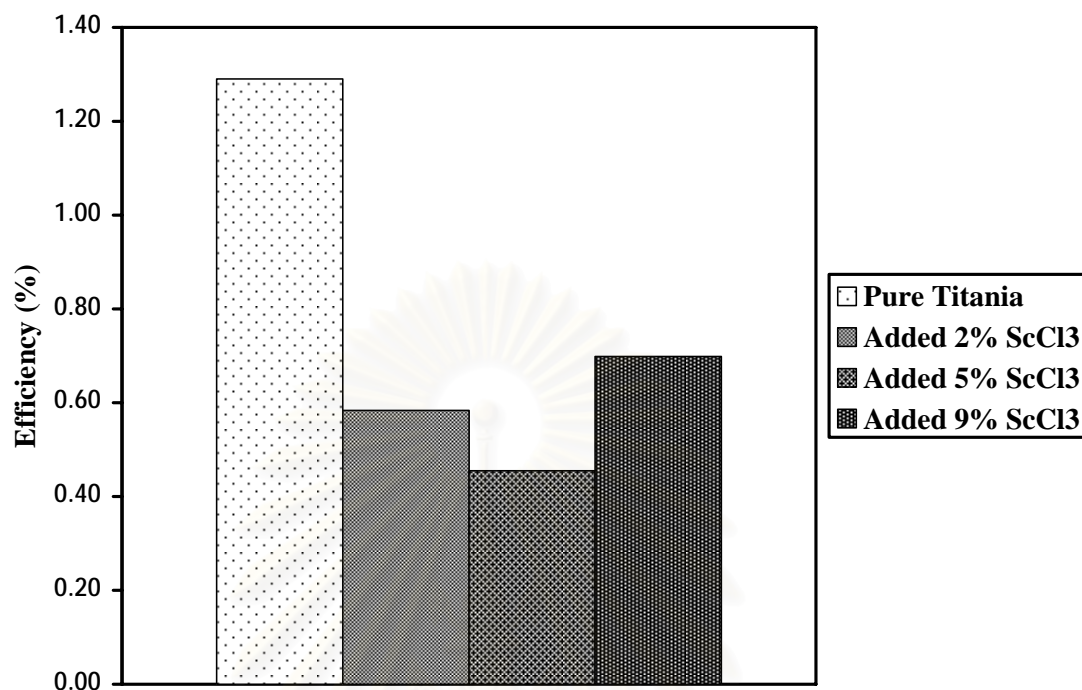


Figure 5.9 Efficiencies of dye-sensitized solar cells with TiO₂ electrode layer modified by scandium at various concentrations.

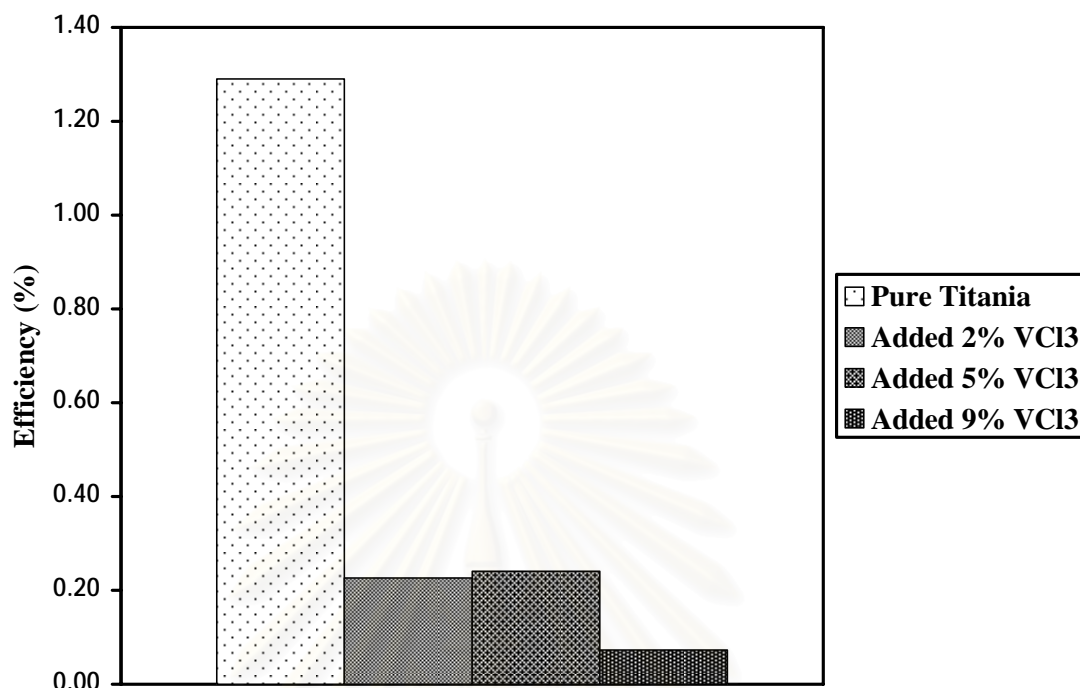


Figure 5.10 Efficiencies of dye-sensitized solar cells with TiO₂ electrode layer modified by vanadium at various concentrations.

Modified TiO₂ sols were used to produce electrode layers for DSSC. The efficiencies of the solar cell with modified TiO₂ electrode layers were measured by an I-V tester and the results are displayed in Figure 5.9 and 5.10. The efficiency of the solar cell dropped significantly upon the addition of scandium and vanadium. The drops may be attributed to increased recombination of electrons and holes in the presence of foreign metals. Kokorin and coworkers [2003] reported that the band gap of polycrystalline TiO₂ doped with vanadium noticeably compared with the initial TiO₂.

5.4.2 Modification of TiO₂ electrode layer by adding TCNQ

TiO₂ sol was modified by adding 7,7',8,8'-tetracyanoquinodimethane (TCNQ) at concentration of 2%, 5%, 9%, 12%, 15% and 19% (w/w). The resulting products were green colloidal mixtures. The modified sol was sprayed on conducting glass until the number of coats reached 150. Grossel and coworkers [2000] stated that TCNQ is a good one-electron acceptor and salts of the resulting radical anion exhibit a wide range of interesting electronic properties including from high electrical conductivity and ferromagnetic behaviour. TCNQ is widely used for improving electrochemical performance of a device [Inzelt, et., 2006; Mandal, et., 2007]. The melting point of TCNQ is 287 °C, at which it also decomposes. The result from thermogravimetric analysis (TGA) for TCNQ in air is displayed in Figure 5.11.

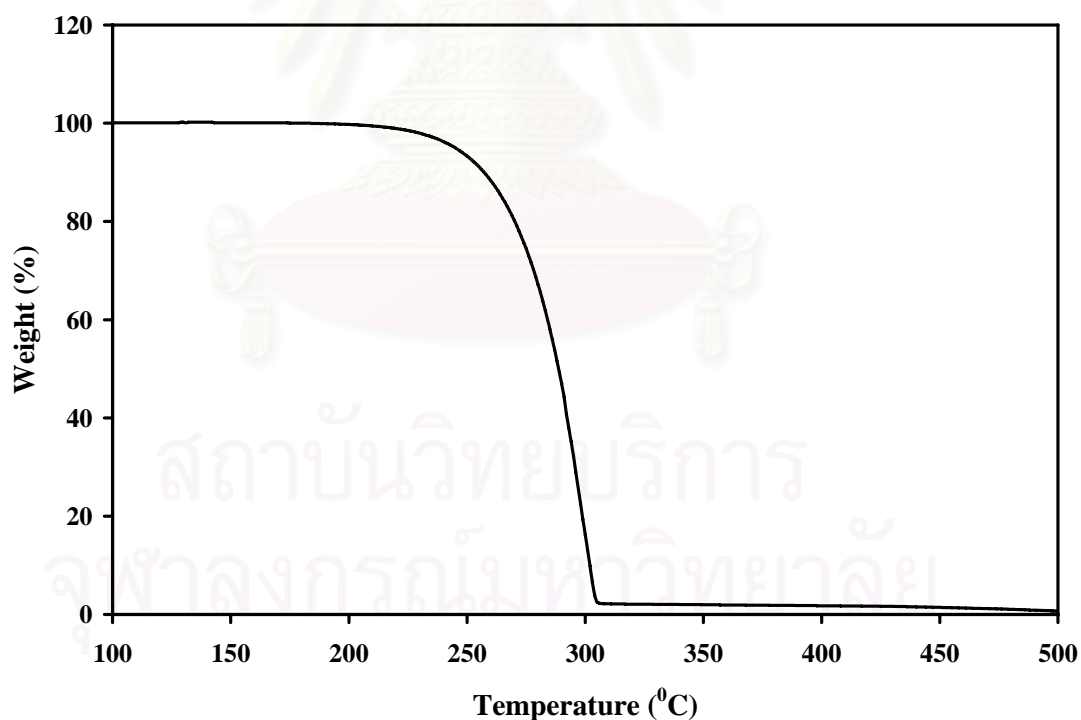


Figure 5.11 Result from thermogravimetric analysis (TGA) for TCNQ in air

From Figure 5.6, TCNQ started decomposing at 250°C and completely disintegrated at 300°C. To retain TCNQ in TiO₂ electrode layer, the sintering temperature for TiO₂ electrode layer was lowered from 400 °C to 250 °C. Electrochemical properties of DSSC with modified TiO₂ electrode layer are listed in Table 5.6.

Table 5.6 Electrochemical properties of DSSC with TiO₂ electrode layer modified by TCNQ at various concentrations.

TCNQ content (%w/w)	V _{OC} (Volt)	J _{SC} (mA/cm ²)	Fill Factor	Efficiency (%)
0%	0.63	1.87	0.51	0.59
2%	0.63	2.55	0.54	0.86
5%	0.62	2.29	0.54	0.76
9%	0.62	2.12	0.53	0.70
12%	0.61	1.82	0.51	0.57
15%	0.67	1.70	0.46	0.53
19%	0.62	1.47	0.48	0.44

Table 5.5 indicated that the open-circuit voltage remained essentially the same after the addition of TCNQ. However, adding TCNQ at 2% (w/w) increased the short-circuit current density to be the highest value at 2.55 mA/cm². Adding more TCNQ resulted in a steady decrease in the short-circuit current density. The increase may be due to the fact that TCNQ improved the electron transfer in TiO₂ thin film [Acker et, al., 1960]. Fill factor and efficiency followed the same trend as the short-circuit current density. The maximum efficiency was obtained from 2% (w/w) TCNQ (see Figure 5.12). The increase were related the increase in J_{sc}.

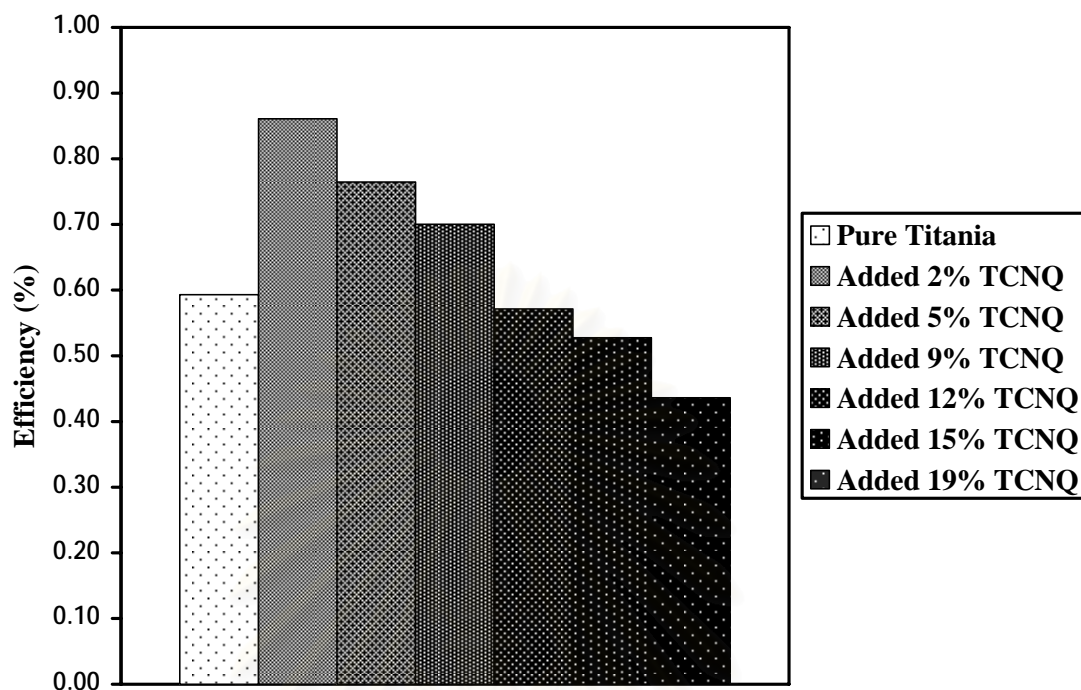


Figure 5.12 Efficiency of dye-sensitized solar cell with TiO_2 electrode layer modified by TCNQ at various concentrations.

5.4.3 Modification of TiO_2 electrode layer with hollow spaces

This study was similar to the study described in section 5.4.2 in the sense that TCNQ was added to TiO_2 sol at concentration of 2%, 5%, 9%, and 15% (w/w). The TiO_2 electrode layer was then fired at 400°C , which exceeded the decomposition temperature of TCNQ (287°C). Therefore, TCNQ completely disintegrated and left behind hollow space where it used to be. The number of coats of TiO_2 layer was 150.

To ascertain whether TCNQ was no longer present in TiO_2 , TCNQ modified TiO_2 samples were characterized by thermogravimetric analyzer (TGA) and Infrared Spectroscopy (FT-IR). The results from TGA (see Figure 5.13) indicated that weight loss patterns for TCNQ modified TiO_2 were similar to that for pure TiO_2 . And no peaks associating with TCNQ were observed in any TCNQ modified samples (see Figure 5.14)

FT-IR spectra of TCNQ modified TiO_2 samples were similar to that of pure TiO_2 . Therefore, TCNQ appear to be absent from all modified TiO_2 that was fired at 400°C .

The electrochemical properties of DSSC with TiO_2 electrode layer modified with hollow spaces are listed in Table 5.6.

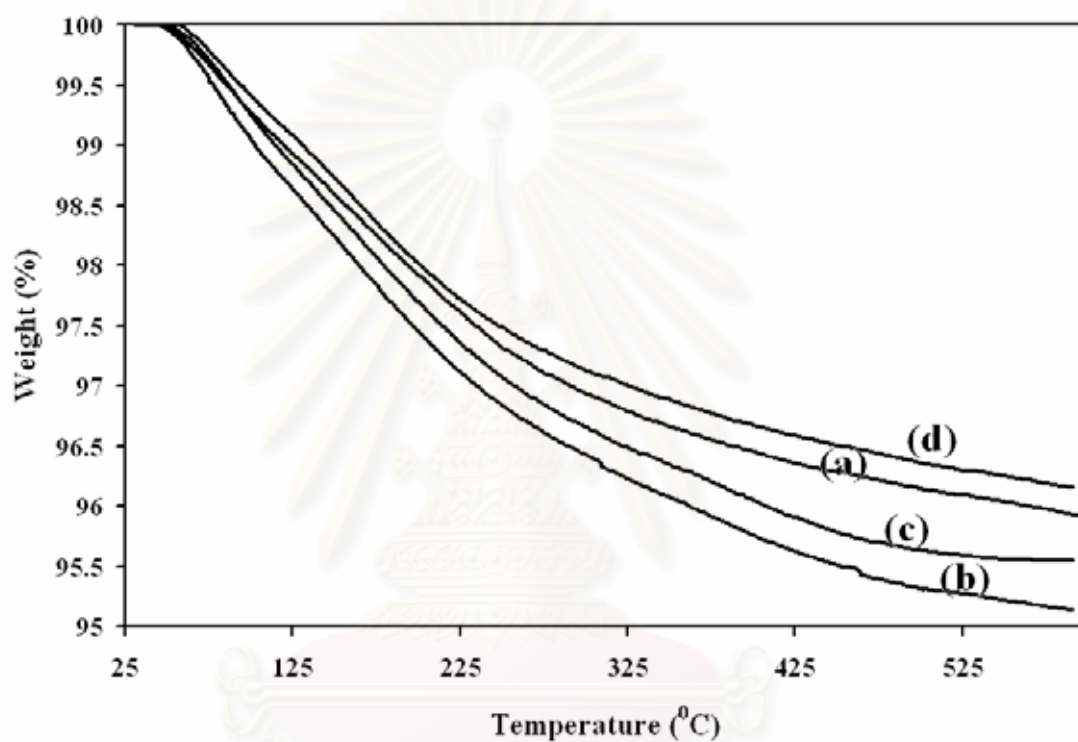


Figure 5.13 Results from TGA for TiO_2 powders that modified by adding TCNQ at (a) 0%, (b) 2%, (c) 5%, and (d) 9% (w/w). The TiO_2 powders were then fired at 400°C .

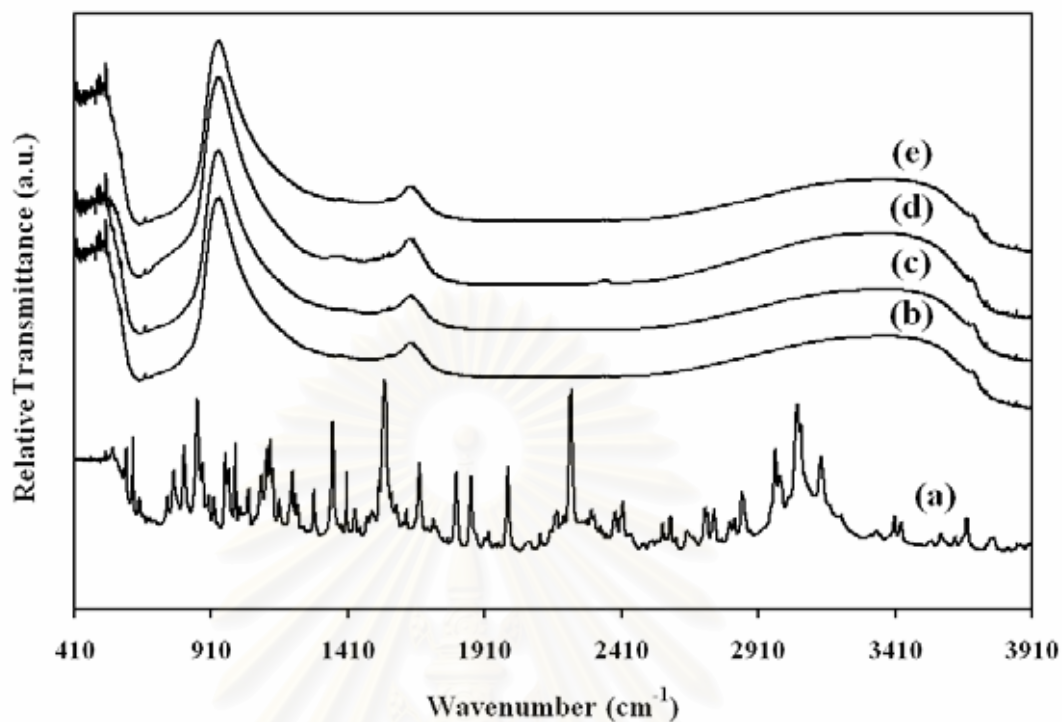


Figure 5.14 Results from FT-IR for TiO_2 powders that modified by adding TCNQ at (a) 0%, (b) 2%, (c) 5%, and (d) 9% (w/w). The TiO_2 powders were then fired at 400°C .

Table 5.7 Electrochemical properties of DSSC with TiO_2 electrode layer modified with hollow spaces derived from TCNQ

TCNQ content (%w/w)	V_{OC} (Volt)	J_{SC} (mA/cm^2)	Fill Factor	Efficiency (%)
0%	0.70	2.47	0.75	1.29
2%	0.71	2.67	0.72	1.33
5%	0.68	2.76	0.73	1.37
9%	0.69	3.11	0.85	1.82
15%	0.67	3.13	0.76	1.63

From Table 5.6, the open-circuit voltage remained essentially unchanged with increasing hollow spaces. However, the short-circuit current density increased from 2.47 mA/cm² to 3.13 mA/cm² when initial concentrations of TCNQ added was raised from 0% to 15% (w/w). Fill factor and efficiency of the solar cells also increased when initial concentrations of TCNQ added was increased up to 9% (w/w). However, drop in both fill factor and efficiency were observed for the solar cell with 15% (w/w) (see Figure 5.15). This from could be a result of adsorbed and aggregated dye molecules inhibiting tri-iodide ions an electrolyte reaching the TiO₂ surface due to steric hindrance [Ko et al., 2004].

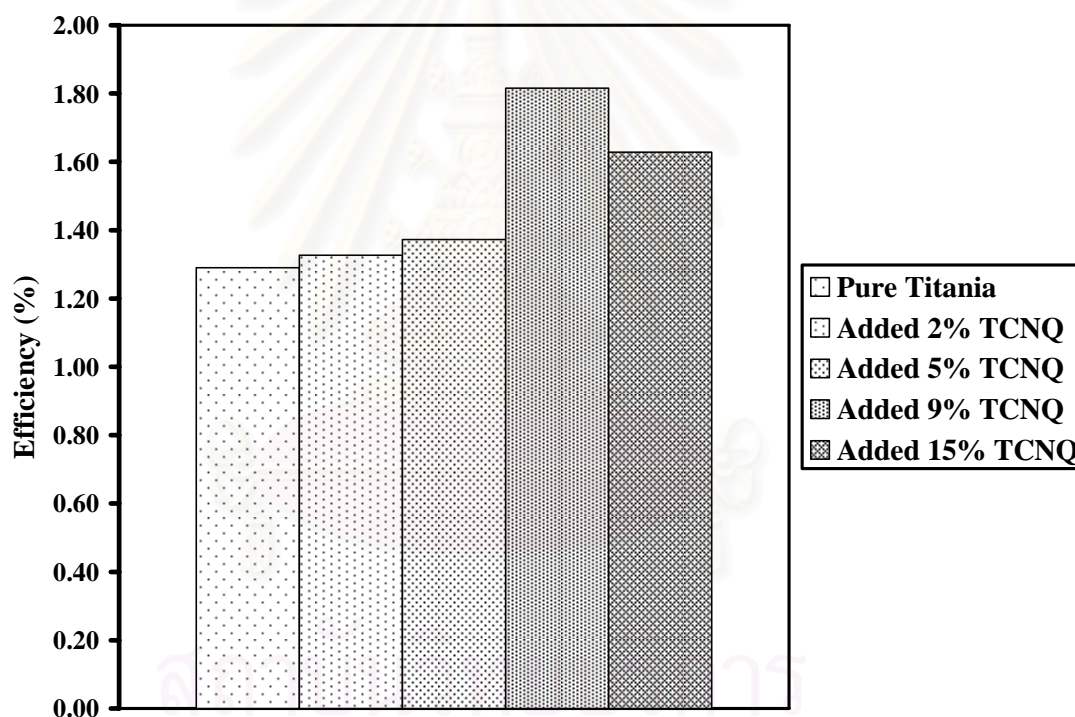


Figure 5.15 Efficiency of dye-sensitized solar cell with TiO₂ electrode layer modified by hollow spaces at various concentrations.

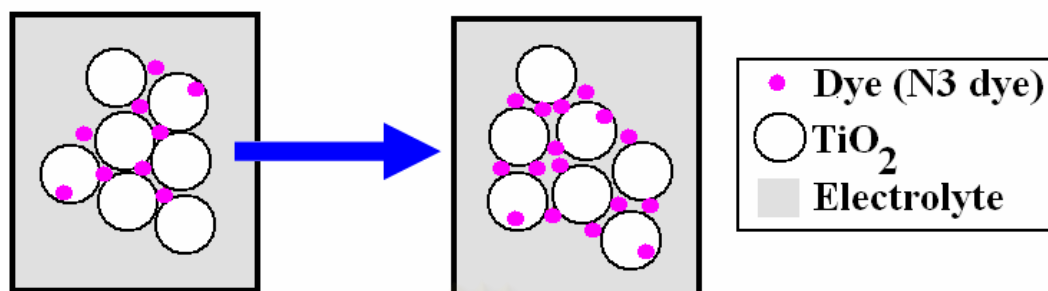


Figure 5.16 Schematic diagram of improved performance of DSSC with TiO₂ electrode layer modified by adding hollow spaces.

From Figure 5.16, this increase in performance of DSSC could be explained by hollow spaces between TiO₂ particles allowing for more absorption of dye and larger space for electron exchange among dye, TiO₂, and electrolyte [Huang et al., 2006].

CHAPTER VI

CONCLUSIONS AND RECOMMENDATIONS FOR FUTURE RESEARCH

Conclusions and recommendations for future research are presented in this chapter.

6.1 Conclusions

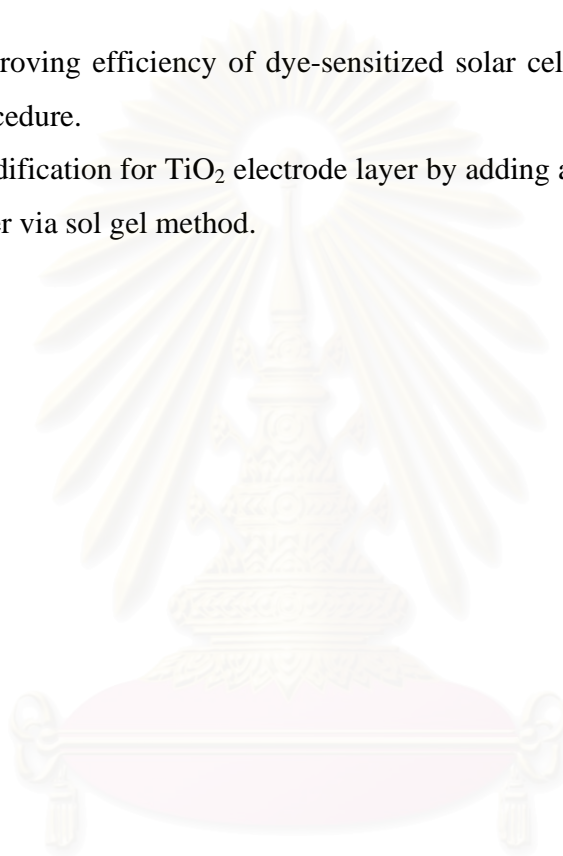
The conclusions of this research are following as:

1. The highest efficiency for DSSC in our study could be obtained when
 - Electrolyte II was used.
 - Sintering temperature for TiO_2 was 500°C (although its I-V curve is not normal).
 - Number of coats of TiO_2 layer was 150.
2. Modification of TiO_2 electrode layer with scandium and vanadium lowered the efficiency of DSSC.
3. Modification of TiO_2 electrode layer with TCNQ could improve the efficiency of DSSC.
4. Addition of hollow spaces (as derived from decomposition of TCNQ, in our case) could enhance the efficiency of DSSC.

6.2 Recommendations for future studies

From the previous conclusions, the following recommendations for future studies are proposed.

1. Improving efficiency of dye-sensitized solar cell by optimizing fabrication procedure.
2. Modification for TiO_2 electrode layer by adding another metal oxide in TiO_2 layer via sol gel method.



สถาบันวิทยบริการ
จุฬาลงกรณ์มหาวิทยาลัย

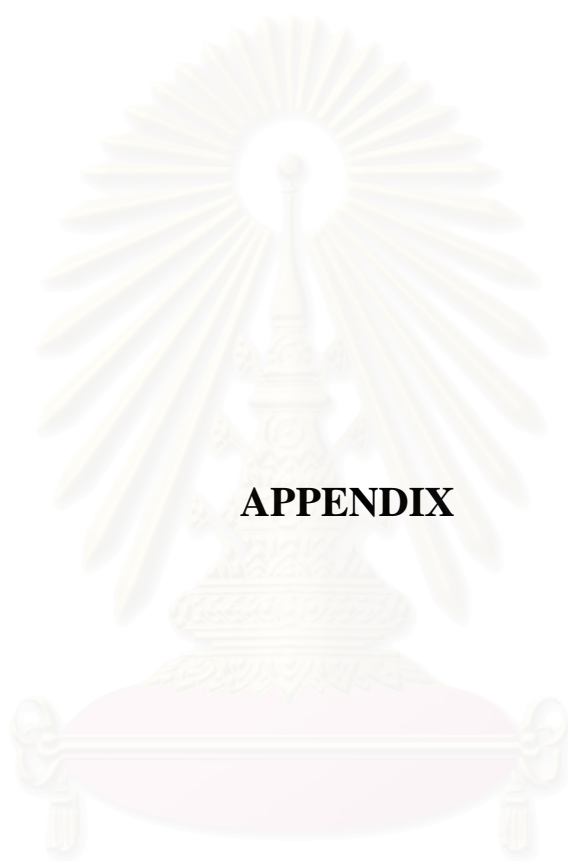
REFERENCES

- Acker, D. S., Harder, R. J., Hertler, W. R., and Mahler, W. 7,7,8,8-Tetracyanoquinodimethane and its Electrically Conducting Antion-Reaical Derivatives. Journal of the American Chemical Society 82 (1960): 1-2.
- Bandara, J., and Weerasinghe, H. Solid-state dye-sensitized solar cell with p-type NiO as a hole collector. Solar Energy Materials & Solar cells 85 (2005): 385-390.
- Fillinger, A., Soltz, D., and Parkinson, B.A. Dye Sensitization of Natural Anatase Crystals with a Ruthenium-Based Dye. Journal of the Electrochemical Society 149 (2002): A1146-A1156.
- Fu, X., Clark, L., Zeltner, W., and Anderson, A. Effects of reaction temperature and water vapor content on the heterogeneous photocatalytic oxidation of ethylene. Journal of Photochem Photobiol A: Chem 97 (1996) 181-186.
- Fujishima, A., Hashimoto, K., and Watanabe, T. TiO₂ photocatalysis: fundamental and applications. 1st ed. Tokyo: BKC, 1999.
- Grätzel, M. Conversion of sunlight to electric power by nanocrystalline dye-sensitized solar cells. Journal of Photochem Photobiol A: Chem 164 (2004): 3-14.
- Grossel, M. C., Duke, A. J., Hibbert, D. B., Lewis, I. K., Seddon, E. A., Horton P. N., and Weston, S. C. An Investigation of the Factors which Influence the Decomposition of TCNQ and its Salts to, and Structural Characterisation of, the alpha,alpha-Dicyano-p-Toluoylcyanide Anion. Journal of Chemistry of Materials 12 (2000): 2319-2323.
- Haraa, K., Nishikawab, T., Kurashigea, M., Kawauchic, H., Kashimac, T., Sayamaa, K., Aikab, K., and Arakawaa, H. Influence of electrolyte on the photovoltaic performance of a dye-sensitized TiO₂ solar cell based on a Ru(II) terpyridyl complex photosensitizer. Solar Energy Materials & Solar Cells 85 (2005): 21–30.
- Hawlicka, E., Grabowski, R., and Bunsenges, B. Self-diffusion in water-alcohol systems 1-Propanol-water solutions of sodium iodide. Journal of Physical Chemistry 94 (1990): 158.

- Huanga, C.Y., Hsua, Y.C., Chena, J.G., Suryanarayanan, V., Leeb, K.M., and Ho, K.C. The effects of hydrothermal temperature and thickness of TiO₂ film on the performance of a dye-sensitized solar cell. Solar Energy Materials & Solar Cells 90 (2006): 2391–2397.
- Inzelt, G., Németh, K., and Róka, A. Electrochemical quartz crystal microbalance study of redox transformations of TCNQ microcrystals in concentrated LiCl solutions. Electrochimica Acta 52 (2007): 4015–4023.
- Kalyanasundaram, K., Gratzel, M., and Coord. Applications of functionalized transition metal complexes in photonic and optoelectronic devices. Chemical Reviews 177 (1998): 347-414.
- Kambe, S., Murakoshi, K., Kitamura, T., Wada, Y., Yanagida, S., Kominami, H., and Kera, Y. Mesoporous electrodes having tight agglomeration of single-phase anatase TiO₂ nanocrystallites: Application to dye-sensitized solar cells. Solar Energy Materials & Solar Cells 61 (2000): 427-441.
- Karthikeyan, C.S., Thelakkat, M., and Willert-Porada, M. Different mesoporous titania films for solid-state dye sensitised solar cells. Thin Solid Films 511 – 512 (2006): 187 – 194
- Kawano, R., and Watanabe, M. Structure and Dynamics of a Confined Ionic Liquid Topics of Relevance to Dye-Sensitized Solar Cells. Chemical Communications (2003) 330.
- Kim, G.S., Seo, H.K., Godble, V.P., Kim, Y.S., Yang, O.B., and Shin, H.S. Electrophoretic deposition of titanate nanotubes from commercial titania nanoparticles: Application to dye-sensitized solar cells. Electrochemistry Communications 8 (2006): 961–966.
- Ko, K. H., Lee, Y. C., and Jung, Y. J. Enhanced efficiency of dye-sensitized TiO₂ solar cells (DSSC) by doping of metal ions. Journal of Colloid and Interface Science 283 (2005): 482–487.
- Kokorin, A. I., Arakelyan, V. M., and Arutyunian, V. M. Spectroscopic study of polycrystalline TiO₂ doped with vanadium. Russian Chemical Bulletin 52 (2003): 93-97.

- Kuang, D., Klein, C., Snaith, H. J., Moser, J. E., Baker, R. H., Comte, P., Zakeeruddin, S. M., and Grätzel, M. Ion Coordinating Sensitizer for High Efficiency Mesoscopic Dye-Sensitized Solar Cells: Influence of Lithium Ions on the Photovoltaic Performance of Liquid and Solid-State Cells. Nano Letters 6 (2006): 769-773.
- Li, Q. S., Ye, B. C., Liu, B. X., and Zhong, J. J. Improvement of the performance of H₂O₂ oxidation at low working potential by incorporating TTF-TCNQ into a platinum wire electrode for glucose determination. Biosensors & Bioelectronics 14 (1999): 327-334.
- Mandal, P., Sahu, T., Misra, T., Pal, S. K., and Ganguly, T. Experimental investigations by using electrochemical, steady state and time resolved spectroscopic tools on the photoreactions of disubstituted indoles in presence of tetracyanoquinodimethane (TCNQ) and a theoretical approach by using time-dependent density functional theory. Journal of Photochemistry and Photobiology A: Chemistry (2007).
- Nelson, J. The Physics of Solar Cells Properties of Semiconductor Materials. 2nd. Singapore: Imperial College Press, 2004.
- Ngamsinlapasathian, S., Sakulphaemaruehai, S., Pavasupree, S., Kitiyanan, A., Sreethawong, T., Suzuki, Y., and Yoshikawa, S. Highly efficient dye-sensitized solar cell using nanocrystalline titania containing nanotube structure. Journal of Photochemistry and Photobiology A: Chem 164 (2004): 145-151.
- O'Regan, B., and Grätzel, M. Low-cost high-efficiency solar cell based on dye-sensitized colloidal TiO₂ films. Nature 353 (1991): 737-740.
- Othmer, K. Encyclopedia of chemical technology. 4th. New York: A Wiley-Interscience Publication, John Wiley&Son, 1991.
- Ramasamy, E., Lee, W. J., Lee, D. Y., and Songa, J. S. Portable, parallel grid dye-sensitized solar cell module prepared by screen printing. Journal of Power Sources 165 (2007): 446-449.
- Redmond, C., and Fitzmaurice, D. Spectroscopic Determination of Flatband Potentials for Polycrystalline TiO₂ Electrodes in Nonaqueous Solvents. Journal of Physical Chemistry 97 (1993): 1426-1430.

- Rothenberger, G., Comte, P., and Grätzel, M. A contribution to the optical design of dye-sensitized nanocrystalline solar cells. Solar Energy Materials & Solar Cells 3 (1999): 321-336.
- Schlaf, R., Parkinson, B. A., Lee, P. A., Nebesny, K. W., and Armstrong, N. R. Absence of final-state screening shifts in photoemission spectroscopy frontier orbital alignment measurements at organic/semiconductor interfaces. Journal of Surface Science 420 (1999): 122-129.
- Shen, Q., Arae, D., and Toyoda, T. Photosensitization of nanostructured TiO₂ with CdSe quantum dots: effects of microstructure and electron transport in TiO₂ substrates. Journal of Photochemistry and Photobiology A: Chem 164 (2004): 75-80.
- Sirisuk, A., Hill, C., and Anderson, M. Photocatalytic degradation of ethylene over thin films of titania supported on glass rings. Catalysis Today 54 (1999): 159-164.
- Su, C., Hong, B., and Tseng, C. Sol-gel preparation and photocatalysis of titanium dioxide. Catalysis Today 96 (2004) 119-126.
- Suri, P., and Mehra, R.M. Effect of electrolytes on the photovoltaic performance of a hybrid dye sensitized ZnO solar cell. Solar Energy Materials & Solar Cells 91 (2007): 518-524.
- Wurfel, P. Physical of Solar Cells from Principles to New Concepts. 1st. Darmstadt: WILEY-VCH Verlag GmbH & Co.KGaA, 2005.



APPENDIX

สถาบันวิทยบริการ
จุฬาลงกรณ์มหาวิทยาลัย

APPENDIX A

CALCULATION OF THE FILL FACTOR AND EFFICIENCY OF DYE SENSITIZED SOLAR CELL

Normally, fill factor and efficiency of solar cell are calculated by software that is installed in the solar simulator (I-V tester). However, when a relationship of current density and voltage is not normal, the fill factor and the efficiency of solar cell should be calculated manually. The efficiency of solar cell can be calculated by the following equation.

$$\eta = \frac{J_{sc} V_{oc} FF}{P_s} \quad (A.1)$$

When:	η	=	Efficiency of solar cell (%)
	J_{sc}	=	Short-circuit current density (mA/cm ²)
	V_{oc}	=	Open-circuit voltage (volt)
	FF	=	Fill Factor (0.0 to 1)
	P_s	=	Power of light source (watt)

A plot of current density and voltage that is obtained from an I-V tester is displayed in Figure A.1.

สถาบันวิทยบริการ
จุฬาลงกรณ์มหาวิทยาลัย

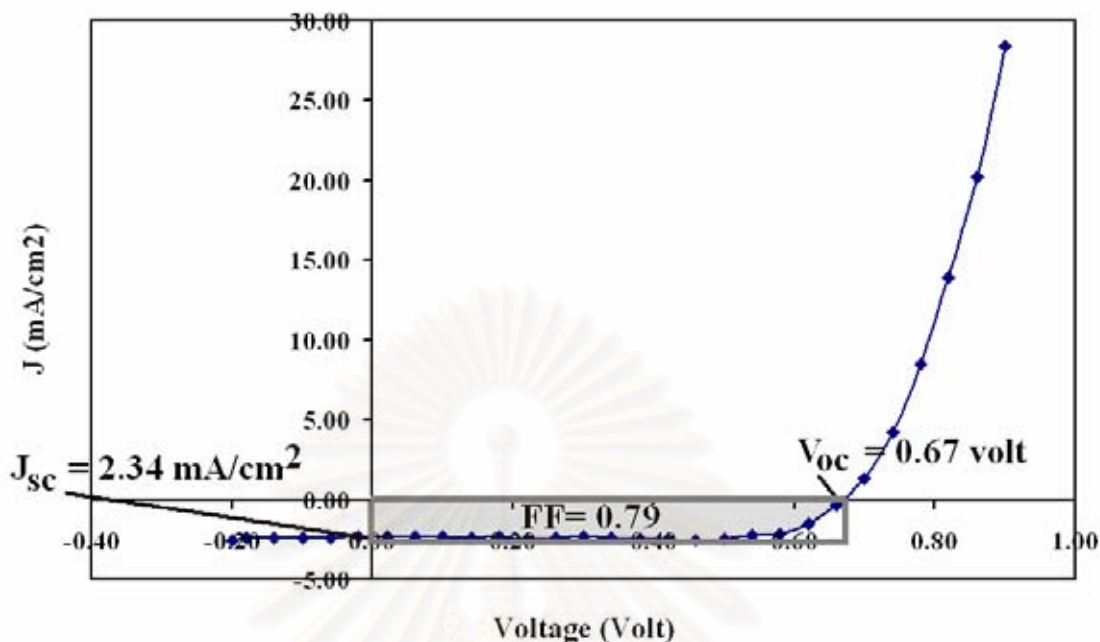


Figure A.1 An I-V curve of DSSC with 150 coats of TiO₂ that is sintered at 400°C.

From Figure A.1, the open-circuit voltage (V_{oc}) is the X axis intercept, and the short-circuit current density (J_{sc}) is the Y axis intercept. The fill factor is the ratio of the shaded area to the area of a rectangle that covers the shaded area. The efficiency can then be calculated using Equation A.1. However, when the I-V curve does not lie parallel to X-axis such as DSSC with TiO₂ layer that is sintered at 500°C (see Figure A.2), an error in the calculation is made since the shaded area is larger than the area of the rectangle. Therefore, the rectangle needs to be redrawn so that the shaded area is contained inside (see Figure A.3). The ratio of the shaded area and the area of the new rectangle can be determined manually. The adjusted fill factor is then used to calculate the correct efficiency from the following equation.

$$\eta_{Corrected} = \eta_{Old} \times \frac{FF_{adjusted}}{FF_{Old}} \quad (A.2)$$

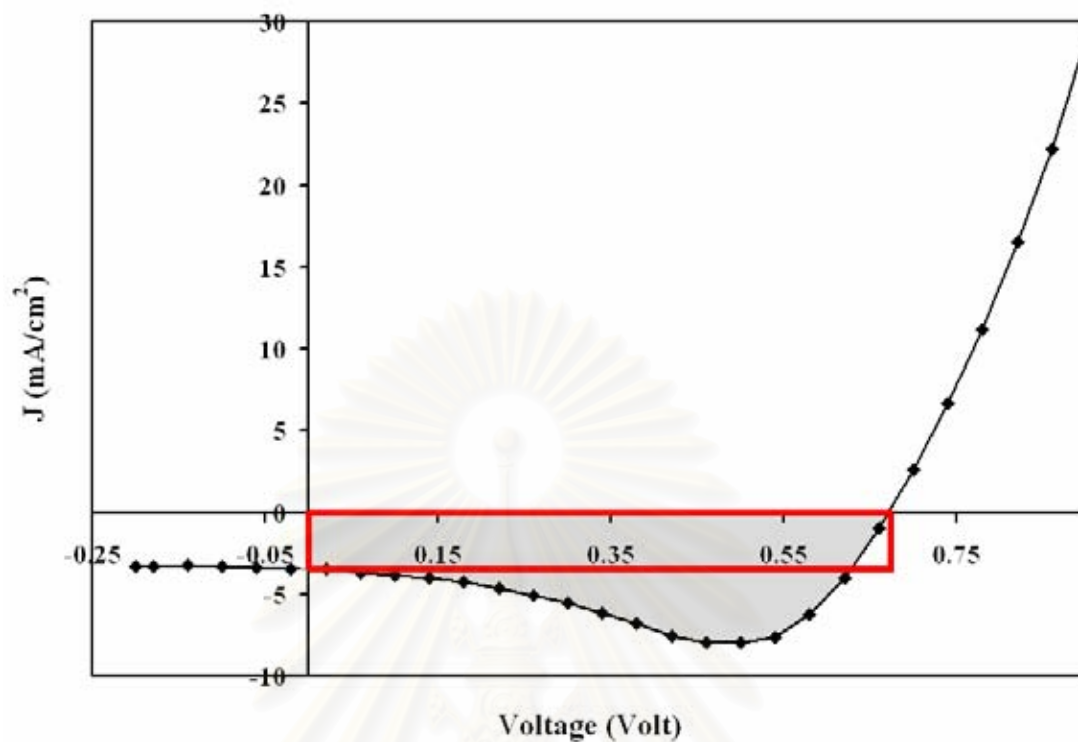


Figure A.2 An I-V curve of DSSC with 180 coats of TiO₂ that is sintered at 500°C.

สถาบันวิทยบริการ
จุฬาลงกรณ์มหาวิทยาลัย

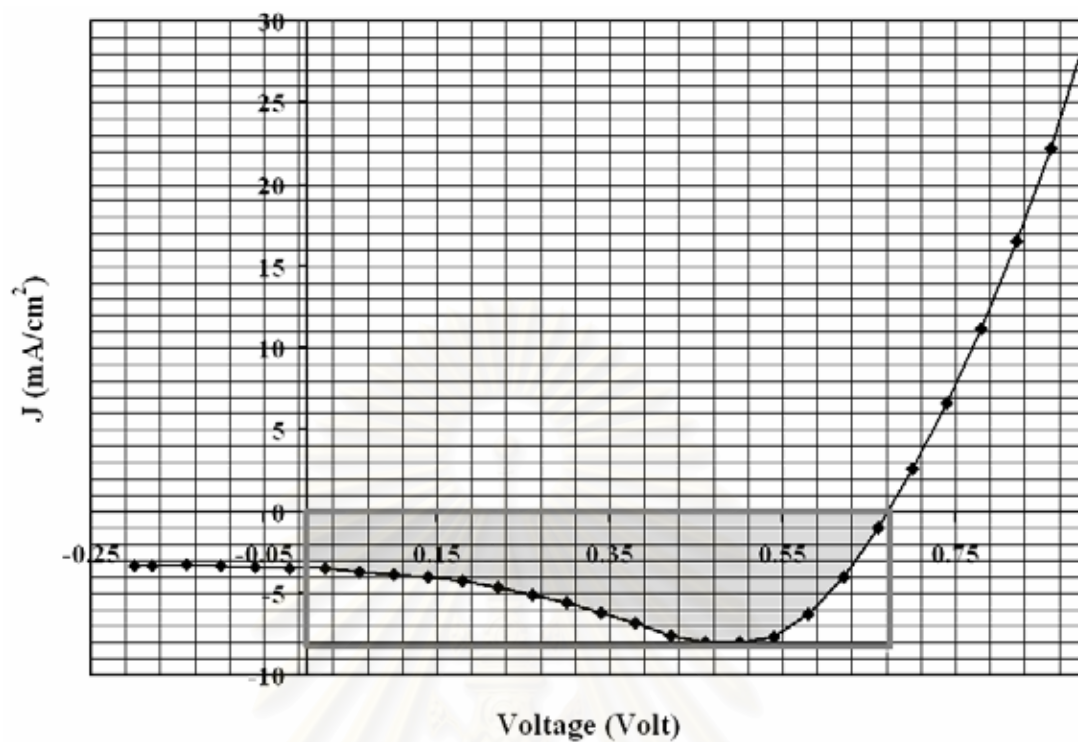


Figure A.3 An I-V curve of DSSC with 180 coats of TiO₂ that is sintered at 500°C. A new rectangle is drawn in order to cover the shaded area.

VITA

Mr. Kulapong Boonyaves was born on February 26, 1982 in Bangkok province, Thailand. He received the Bachelor Degree of Chemistry from Faculty of Science, King's Mongkut University of Technology Thunburi, in 2003. He pursued his Master's study at Chulalongkorn University in June, 2005.



สถาบันวิทยบริการ
จุฬาลงกรณ์มหาวิทยาลัย